Cobalt based layered perovskites as cathode material for intermediate temperature Solid Oxide Fuel Cells: A brief review

Renato Pelosato*, Giulio Cordaro, Davide Stucchi, Cinzia Cristiani, Giovanni Dotelli

Politecnico di Milano, Dipartimento di Chimica Materiali e Ingegneria Chimica "G. Natta", Piazza Leonardo da Vinci 32, 20133 Milano, Italy

Received 16 June 2015
Received in revised form
7 August 2015
Accepted 9 August 2015
Available online xxx

1. Introduction

Solid Oxide Fuel Cells (SOFCs) represent one of the most promising technology for clean energy production, because of a combination of high efficiency, high energy and power densities and fuel flexibility. SOFCs convert the chemical energy of a fuel into electrical energy through redox reactions. Conventional SOFCs must operate at high temperature (~1000 °C) to obtain the required performance. This high operating temperature leads to degradation of fuel cell elements, interfacial reactions among the components, and limits the choice of materials that can be used. Therefore, decreasing the operating temperature of SOFCs from the traditional ~1000 °C to the Intermediate Temperature (IT) range of 500–700 °C would reduce several drawbacks, such as short lifetime of the materials, high system and operating costs and limited material selection. One of the main advantages of decreasing the operating temperature is the opportunity to use metallic interconnections inside the cell, instead of the more expensive and brittle ceramic materials.

* Corresponding author.
E-*mail address:* renato.pelosato@polimi.it (R. Pelosato).

2. IT-SOFC materials

2.1. Electrolyte

The most well-established part of IT-SOFC is the electrolyte [1,2]. Most of the research on electrolyte materials has been devoted to oxygen ion conductors (opposed to proton conductors [3]), and Yttria-Stabilized Zirconia (YSZ) was first selected and extensively used in high temperature SOFCs; by the way, being the ionic conductivity a thermally activated process, lowering the operating temperature reduces the electrolyte performance. Therefore, alternative materials are needed for operation in the intermediate temperature range. The most important requisite for an electrolyte material is a high ionic conductivity, in order to transfer O^{2-} ions towards anode section, but YSZ show high conductivity only at high temperature. Alternative electrolytes for IT-SOFC with fluorite structure are based on cerium oxide. The best performance has been achieved with gadolinium or samarium as dopants, and GDC ($Ce_{1-x}Gd_xO_2$) and SDC ($Ce_{1-x}Sm_xO_2$) are nowadays recognized as suitable intermediate temperature electrolytes. Another electrolyte for IT-SOFCs is $La_{1-x}Sr_xGa_{1-y}Mg_yO_{3-(x+y)/2}$, generally referred to as LSGM. Although it exhibits high oxygen ion conductivity, LSGM is less used than their fluorite counterparts because of many issues concerning the reactivity with the electrode materials and the difficulties in obtaining the material as a pure phase.

2.2. Anode

The anode is the part of the fuel cell where the fuel is oxidized and releases its electrons. Anodic materials need to be a good catalysts for fuel oxidation and good electronic conductors to provide a path for the electrons to the external circuit. In addition, a Thermal Expansion Coefficient (TEC) value comparable to that of the common electrolytes is required. The most used anode material in SOFCs and IT-SOFCs is Ni-YSZ cermet [4]. Nevertheless, the Ni component has some weaknesses such as particle coarsening during operation, thermal expansion mismatch with YSZ, and suffers from carbon deposition; also other cermets have been studied, such as Cu-GDC ($Ce_{1-x}Gd_xO_2$). Recently, the use of perovskite materials in the anode side has raised some interest [5]; the most promising compounds are $La_{0.75}Sr_{0.25}Cr_{0.5}Mn_{0.5}O_3$ (LSCM) [6] and strontium molybdates such as Sr_2MnMoO_6 and Sr_2NiMoO_6 [7]. However, the activity of perovskites significantly drops at temperatures below 700 °C.

2.3. Cathode

Nowadays, the cathode is the most studied component in IT-SOFCs. This happens because the cathodic reaction usually requires a very high activation energy; decreasing SOFCs operating temperature implies slower kinetics of the oxygen reduction reaction and therefore causes a significant drop in fuel cell performance. Hence, extensive researches have been carried out on new cathodic materials, in order to improve the cell efficiency in the intermediate temperature range. There is a general agreement in the scientific community that in order to maximize the performance in the intermediate temperature range, cathode materials need to hold mixed ionic–electronic conductivity properties, i.e. they shall be Mixed Ionic–Electronic Conductors (MIECs). Since the Oxygen Reduction Reaction (ORR) is the step with highest activation energy, decreasing the operating temperature causes a large electrical loss at the cathode. The reaction requires the direct contact of three different phases: gas (oxygen), electrode and electrolyte. This interface is called Three-Phase Boundary (TPB) and in pure electronic conductor cathodes it is limited to a thin region at the electrolyte surface, which extension is mainly determined by the morphologic structure of the cathode. MIECs instead, thanks to their oxygen ion conductivity, allow the diffusion of oxygen ions through the whole cathode layer; thus, this interface is extended to all the contact points between the gas and solid phase.

Since the conventional cathode for high temperature SOFCs is LSM ($La_xSr_{1-x}MnO_3$), similar perovskite materials have been widely studied. The first materials to be investigated were lanthanum manganite, cobaltite and ferrite based materials. Also other solid oxides have been studied as alternative of simple perovskites, such as Ruddlesden–Popper series (RP) and double perovskites as examples [5]. However, there is still no obvious solution to the quest for optimized IT-SOFC cathode material.

RP oxides present general formula $A_{n+1}A'_2B_nO_{3n+1}$ and consist of $n$$ABO_3$ perovskite layers between two A′O rock-salt layers. In particular, materials with $n = 1$ exhibit a mixed ionic and electronic conductivity, appropriate electrochemical activity and suitable chemical and mechanical compatibilities with other SOFC components. This class of the RP family adopts the K_2NiF_4-type structure and results of particular interest for several solid electrolyte applications [8]. Among the materials with this structure, the RE_2MO_4 series (with *RE* = rare earths and M = transition metals) presents the best electrochemical performance [9].

Double perovskites are compounds with general formula $AA'B_2O_{5+\delta}$ and they are composed of alternate layers of single perovskite $ABO_{3-\delta}$ and $A'BO_{3-\delta}$. Several manganite, cobaltite or ferrite based compounds can adopt the layered structure and indeed many composition have been prepared and characterized [10].

For an exhaustive discussion of the general topic of cathode materials in SOFCs, the reader is referred to the reviews by Tsipis & Kharton [10–12], while in the next sections of this paper, the authors will give an overview of the class of double perovskite compounds.

3. $AA'B_2O_{5+\delta}$ double perovskites as cathodes

3.1. General overview

Recently, double perovskites have become attractive structures for application in IT-SOFCs, demonstrating very good electrochemical performance. In particular, double perovskites in which a Rare Earth (*RE*) ion occupy the A site, barium the A′ site and cobalt the B site, have received increasing consideration, thanks to their high of oxygen vacancies concentration, high electronic conductivity and catalytic activity. Their general formula is $REBaCo_2O_{5+\delta}$. Tarancon and co-workers [13] recently summarized the findings of the previous studies. Since then, an increasing interest has born about double perovskite materials, especially for the cobalt containing ones; particular efforts have been devoted to develop effective doping strategies, with the aim of improving the electric, electrochemical or thermal expansion characteristics of these compounds, in order to fit the requirements of IT-SOFC cathode materials.

This increasing interest for double perovskite materials has been driven by the discovery that a perovskite structure offers a remarkable enhancement of the oxygen diffusivity when elements are ordered in alternate layers along the *c* axis of the lattice. In fact, the regular layers of double perovskites reduce the oxygen bonding strength and generate channels that ease the ion motion [14]. In order to obtain the desired regularly stacked structure, the choice of the composition of a double perovskite has to be properly made; the main involved driving force are the ionic radii of the elements that constitute the compound. It is fundamental that the difference between the ionic radii of the elements occupying A and A′ site is

significant, otherwise the two cations will randomly distribute in a disordered A(A′)BO_3 lattice.

As mentioned above, rare earth elements usually occupy the A site in a typical double perovskite. In A′ site an element with appropriate dimension is required, and big ions such as barium or strontium were proposed.

Transition metals are situated in the B site. The most used ones are cobalt, manganese, iron and copper; Co based double perovskites (*RE*$BaCo_2O_{5+\delta}$) were found to usually offer the highest catalytic activity [15–17]. One of the reasons is that this class of compounds can accept a large amount of oxygen vacancies (oxygen concentration $5 \leq 5 + \delta \leq 6$), driven by the mean Co oxidation state; the oxygen content in the final material has also a correlation with the size of the A and A′ cations and can also be governed by the annealing conditions. A linear relationship has been reported between the oxygen content and A site ionic radii difference [r(A) − r(A′)] [17]. As the size of the A cation decreases, the mean oxygen content at room temperature decreases, according to Anderson et al. and Maignan et al. [18,19]. According to the data collected in this review, the reported values for the undoped compounds are: 5.80–6.00 for $LaBaCo_2O_{5+\delta}$, 5.64–5.89 for $PrBaCo_2O_{5+\delta}$, 5.62–5.85 for $NdBaCo_2O_{5+\delta}$, between 5.31 and 5.51 for $YBaCo_2O_{5+\delta}$, 5.40–5.69 $SmBaCo_2O_{5+\delta}$, 5.40–5.66 for $GdBaCo_2O_{5+\delta}$, 5.40–5.52 in $EuBaCo_2O_{5+\delta}$ and 5.40 in $TbBaCo_2O_{5+\delta}$, down to approximately 5.30–5.36 for $DyBaCo_2O_{5+\delta}$ and 5.14–5.30 in $HoBaCo_2O_{5+\delta}$. The relative ionic radii of the two A site cations also drive the structural transitions; According to Kim and Manthiram [20] a disordered structure is obtained when large rare earth ions such as La are used. Thus, La-based perovskites can be considered as doped simple perovskite with general formula $A_{0.5}A'_{0.5}BO_3$; this is confirmed by the fact that La-based compounds are usually indexed in a cubic lattice.

In addition, the unit cell volume increases with rare earths dimension as Co ions are driven to adopt the electronic configuration that minimizes their ionic size [20]. When increasing the oxidation state from Co^{3+} to Co^{4+} the ionic radius of Co decreases, inducing Co to adopt 3.5 oxidation state (i.e. 6 oxygen moles). This indicates a lack of oxygen vacancies, that hinders ionic conductivity and reduces oxygen reduction activity. Nonetheless, the ordered structure has been also achieved in lanthanum compounds by some authors, by carefully tailoring the annealing conditions [21]. Another issue in La-based perovskites is the high TEC value, caused by elevated ionicity of the La–O bonds; a TEC $= 24.3 \cdot 10^6\ K^{-1}$ [20] is reported.

At the opposite side, when the size difference between Ba and *RE* cation is high, the ordered structure is obtained. This usually leads to a reduction of the electrical conductivity, as the high concentration of oxygen vacancies is thought to cause a distortion of O–Co–O bonds, hampering the conduction mechanism [22]. Compounds like $YBaCo_2O_{5+\delta}$ and $HoBaCo_2O_{5+\delta}$ are sensitive to decomposition in air atmosphere at high temperatures [23], but can be stabilized by releasing the size difference with proper doping [24]. However, several researchers investigated these compounds [24,25], because those elements allow obtaining low TECs [20].

The most common crystal structure obtained for double perovskite compounds is tetragonal, but some papers report an enhanced distortion of the lattice structure that leads to orthorhombic lattices. This distortion is related to the oxygen content [18,20]. Anderson et al. [18] suggest that oxygen content is the fundamental parameter for the structure arrangement of the *RE*$BaCo_2O_{5+\delta}$ series; varying the oxygen content in the $NdBaCo_2O_{5+\delta}$ compound by annealing in controlled atmosphere allowed obtaining different crystal structures. Although $NdBaCo_2O_{5+\delta}$ usually presents a tetragonal structure, compositions with oxygen contents between 5.25 and 5.6 adopted an orthorhombic arrangement. Chavez et al. [26] revealed how cooling rate plays a dominant role. Also, it was possible to obtain $GdBaCo_2O_{5+\delta}$ [27] and $YBaCo_2O_{5+\delta}$ [28] with either tetragonal or orthorhombic lattice by controlling the synthesis conditions.

3.2. Summary of available data

In this section, the authors will mainly focus on a few electrochemical and thermal parameters to compare the investigated cathode materials: total electrical conductivity, area specific resistance (ASR), activation energy ($E_{act.}$) and thermal expansion coefficient (TEC). For sake of completeness, also oxygen content, lattice cell parameters, synthesis method, and other available data have been collected and reported. Then the focus will be on a few selected ones (Section 4), and on doping strategies (Section 5).

The relevant physical, chemical and electrochemical parameters are reported in the following tables for several compounds. The total electric conductivity [$S \cdot cm^{-1}$], ASR [$\Omega \cdot cm^2$], activation energies [eV] and thermal expansion coefficients [$10^6\ K^{-1}$] obtained from literature are reported. The relevant chemical and physical parameters like preparation method, sintering temperature, lattice type and cell parameters, oxygen content are also reported for the same compounds.

Table 1 reports some selected electrochemical and thermal parameters of La-based compounds; Table 2 reports other relevant chemical and physical parameters and the preparation method and temperature for the same compounds.

In La-Based compounds, the highest electrical conductivity is obtained in the disordered compound with the cubic structure (Tables 1 and 2, Ref. [20]), while for La-based ordered perovskites much lower values are reported, sharply enhanced only in the Cu-doped compounds [31]. ASR measurements are available only in the work by Zhang et al. [29] and are quite high respect to other compounds reported below, despite the evidence of the ordered structure and the presence of oxygen vacancies (oxygen content = 5.80, Table 2, Ref. [29]).

Table 3 reports some selected electrochemical and thermal parameters of Pr-based compounds; Table 4 reports other relevant chemical and physical parameters and the preparation method and temperature for the same compounds.

It is quite challenging to draw conclusions comparing Pr-based compounds; a lot of efforts have been devoted to synthesize and characterize those compounds, with doping in either A or B sublattices, and very diverse results have been obtained. Generally, electrical conductivity values are the highest among the series and the ASR are the lowest, except for those compounds doped with iron or scandium on cobalt site (Table 3). Also many of the compounds bearing iron or scandium are found to adopt a cubic structure, as if those elements promote an ordering of the lattice. The reported oxygen contents spread in the 5.29–6.00 range, even if the lowest values are obtained when Pr is partially substituted by Y ([36]). Thermal expansion coefficients of these compounds can range from $15.2 \cdot 10^6\ K^{-1}$ [43] for Cu doped compound up to $26 \cdot 10^6\ K^{-1}$ [39] but mainly show values around $20 \cdot 10^6\ K^{-1}$.

Table 5 reports some selected electrochemical and thermal parameters of Nd-based compounds; Table 6 reports other relevant chemical and physical parameters and the preparation method and temperature for the same compounds.

Also in the case of Nd-based compounds, it is worth noting the large spread of measured electrical conductivity values (see Table 5, Refs. [20] and [29] for an example regarding the undoped compounds). Very high values are often reported for Sr-doped compounds. Similarly to what happens in Pr-based compounds, iron doping seem to promote a change of the structure towards a

Table 1
Composition, electrical conductivity σ, ASR, activation energy and TEC of La-based double perovskite cathodes.

Composition	σ @ 600 °C [S·cm^{-1}]	σ @ 700 °C [S·cm^{-1}]	ASR @ 600 °C [Ω·cm^2]	ASR @ 700 °C [Ω·cm^2]	E act. [eV]	TEC [10^6 K^{-1}]	Reference
$LaBaCo_2O_{5+\delta}$	1443	1076	–	–	–	24.3	[20]
$LaBaCo_2O_{5+\delta}$	60.0	52.2	3.56	0.56	–	–	[29]
$LaBaCo_2O_{5+\delta}$	459	457	–	–	–	–	[30]
$LaBaCuCoO_{5+\delta}$	392	345	–	–	–	–	[31]
$LaBaCuFeO_{5+\delta}$	123	93.7	–	–	–	–	[31]
$LaSrMnCoO_{5+\delta}$	111	124	–	–	–	15.8	[32]

Table 2
Composition, synthetic route, sintering temperature, lattice type and parameters and oxygen content of La-based double perovskite cathodes. SS = Solid state; SG = Sol-Gel; C = Combustion; P = Pechini.

Composition	Synthesis method	Sintering temp [°C]	Lattice type	*a* [Å]	*b* [Å]	*c* [Å]	Oxygen content[5+δ]	Reference
$LaBaCo_2O_{5+\delta}$	SS	1100	C	3.940	–	–	6.00	[33]
$LaBaCo_2O_{5+\delta}$	SS	1100	C	3.881	–	–	6.00	[20]
$LaBaCo_2O_{5+\delta}$	SG	1150	O	3.898	3.891	7.718	5.80	[29]

disordered cubic with higher oxygen contents (see for example Ref. [56]). ASR as low as 0.04 Ω cm^2 are reported at 700 °C (Table 5 [29], [55]) for the undoped compound, probably as a result of the very effective oxygen surface exchange activity [60]. Oxygen content ranges between 5.62 and 5.85 for $NdBaCo_2O_{5+\delta}$ and extends to 5.23–6.00 if we take into account all the reported compositions, some of which are anyway annealed in strong reducing or oxidizing environments.

Table 7 reports some selected electrochemical and thermal parameters of Sm-based compounds; Table 8 reports other relevant chemical and physical parameters and the preparation method and temperature for the same compounds.

Conductivity differences in the reported $SmBaCo_2O_{5+\delta}$ compounds are quite high (see Table 7, Ref. [20] and [29]). Largely, high conductivity values (>100 S cm^{-1}) are reported except for Mn bearing compounds where it is significantly lower (Table 7, Ref. [64]). The lowest reported ASR values are 0.10 Ω cm^2 at 700 °C for $SmBaCo_2O_{5+\delta}$ (Table 7, Ref. [63]) and 0.07 Ω cm^2 in $SmSrCo_2O_{5+\delta}$ (Ref. [64]). Oxygen contents of 5.40–5.69 are reported for undoped $SmBaCo_2O_{5+\delta}$ while it extends to 5.36–6.00 taking into account the doped compounds. Despite the poor conductivities obtained, the samples doped with manganese allow lowering the TEC values, down to about 13.8·10^6 K^{-1} (Table 7, Ref. [64]).

Table 9 reports some selected electrochemical and thermal parameters of Gd-based compounds; Table 10 reports other relevant chemical and physical parameters and the preparation method and temperature for the same compounds.

Gd-based compounds seem to grant very low ASR values in some compositions (Table 9, Refs. [27,29,71]) while the reported conductivities reach the highest values only in Sr-doped compounds (Table 7, Refs. [67,73]) while the double doping with Sr- and Fe-dampens the conductivity again (Table 7 Refs. [74,73]). The reported TEC values are in many references considerably lower respect to the values of analogous Pr-, Nd- and Sm-based samples. Except for the very high values reported in Refs. [56] and [67] (i.e. 6.00 and 5.98) the oxygen content range is 5.40–5.83 mol of oxygen per mole of compound.

Table 11 reports some selected electrochemical and thermal parameters of Y-based compounds; Table 12 reports other relevant chemical and physical parameters and the preparation method and temperature for the same compounds.

As already mentioned, the undoped $YBaCo_2O_{5+\delta}$ is prone to decomposition by simply heating the sample at high temperature in air, but its structure can be stabilized by proper doping [24]; focusing on doped compounds, it is worth noting that the electrical conductivity values are much lower than those of Pr- and Nd-based counterparts, and only a few composition cross the threshold of 100 S cm^{-1} (Table 11, Refs. [25,76], and in a minor extent Refs. [77,79]). Except for the results of Zhang et al. (Table 12, Ref. [29]) all the reported Y-bearing compounds adopt a tetragonal lattice. A few measurements are available of the oxygen content, that is indeed significantly lower than in the other examined rare earth double perovskites (= 5.31–5.51).

For sake of completeness, Table 13 reports the relevant chemical and physical parameters: preparation method, sintering temperature, lattice type and cell parameters, oxygen content for other minor rare earths based compounds, for which electrochemical measurements are not reported.

As mentioned above, A site cation dimension is understood to have an influence on the crystal structure and on the electrochemical properties: at a first sight, it can be stated that the best performance are obtained when middle-sized ions occupy the A site (praseodymium, neodymium, samarium and gadolinium); in Table 14 the ionic size of the investigated A site cations are reported, as the effective ionic radius of the 12-fold coordinated ion when available, or as the size of the 9-fold coordinated ion [80,81]. In the end, it appears that these elements provide a good trade-off between electrochemical activity and TEC. This is not surprising, as it has been shown that both TEC and electrical conductivity generally decrease reducing the size of the rare earth ion in $REBaCo_2O_{5+\delta}$ [20]. Thus, a detailed analysis has been performed on the compounds with the mentioned elements on the A site. However, also Y-based compounds look quite promising in some compositions, because they keep the lowest TEC values in the series, which better mimic the thermal expansion coefficients of the common intermediate temperature electrolytes.

The analysis of the results reported in the available literature faces a complication that somehow hinders the understanding of the key factors affecting the effectiveness of cathodic materials. This issue is the high spread of results, especially in term of conductivity and ASR results reported for homologous compounds. From Tables 1–3, it is noticeable that the same compound, synthesized by different researchers or under slight different conditions, often shows very dissimilar values of the relevant electrochemical parameters. To put this fact in better evidence, Fig. 1 shows a general overview of all the electric conductivity values reported for the investigated compounds. They are grouped by the A site rare earth: Pr, Nd, Gd, Sm and Y respectively. For each A site element, conductivity values are reported for every composition, split in quartiles: 50% of the intermediate values are shown

Table 3
Composition, electrical conductivity σ, ASR, activation energy and TEC of Pr-based double perovskite cathodes.

Composition	σ @ 600 °C [S·cm^{-1}]	σ @ 700 °C [S·cm^{-1}]	ASR @ 600 °C [Ω·cm^2]	ASR @ 700 °C [Ω·cm^2]	E act. [eV]	TEC [10^6 K^{-1}]	Reference
$PrBaCo_2O_{5+\delta}$	–	–	–	–	0.95	21.5	[34]
$PrBaCo_2O_{5+\delta}$	894	730	–	–	–	–	[35]
$PrBaCo_2O_{5+\delta}$	–	–	–	–	–	21.5	[36]
$PrBaCo_2O_{5+\delta}$	844	695	–	0.75	–	20.4	[37]
$PrBaCo_2O_{5+\delta}$	–	–	0.18	0.04	1.19	–	[38]
$PrBaCo_2O_{5+\delta}$	–	–	13.2	0.67	–	–	[26]
$PrBaCo_2O_{5+\delta}$	161	141	0.21	0.02	–	24.1	[29]
$PrBaCo_2O_{5+\delta}$	214	172	–	–	–	24.6	[39]
$PrBaCo_2O_{5+\delta}$	–	–	1.83	0.21	–	–	[40]
$PrBaCo_2O_{5+\delta}$	392	364	0.87	0.18	–	–	[41]
$PrBaCo_2O_{5+\delta}$	588	437	0.12	–	–	–	[42]
$PrBaCoCuO_{5+\delta}$	144	124	0.21	0.05	–	15.2	[43]
$PrBaCoFeO_{5+\delta}$	204	163	–	–	–	21.0	[44]
$PrBaCoFeO_{5+\delta}$	–	–	–	–	–	21.0	[34]
$PrBaCoFeO_{5+\delta}$	72.8	65.3	1.69	0.28	–	–	[41]
$PrBaFe_2O_{5+\delta}$	9.2	7.1	–	–	–	17.2	[39]
$PrBaFe_2O_{5+\delta}$	25.4	22.7	2.76	0.48	–	–	[41]
$PrSrCo_2O_{5+\delta}$	2084	1776	0.19	–	0.93	–	[42]
$PrBaCo_{1.0}Fe_{1.0}O_{5+\delta}$	91.8	68.4	–	–	–	25.0	[39]
$Pr_{0.3}Y_{0.7}BaCo_2O_{5+\delta}$	414	420	1.25	0.18	–	–	[36]
$Pr_{0.5}Y_{0.5}BaCo_2O_{5+\delta}$	582	564	1.46	0.20	–	17.2	[36]
$Pr_{0.7}Y_{0.3}BaCo_2O_{5+\delta}$	730	649	0.90	0.12	–	17.6	[36]
$PrBa_{0.5}Sr_{0.5}Co_2O_{5+\delta}$	–	–	0.08	0.02	–	–	[45]
$PrBa_{0.5}Sr_{0.5}Co_2O_{5+\delta}$	998	818	–	0.09[a] 0.19[b]	–	–	[46]
$PrBa_{0.5}Sr_{0.5}Co_2O_{5+\delta}$	–	–	0.85	0.44	1.23	–	[47]
$PrBa_{0.5}Sr_{0.5}Co_2O_{5+\delta}$	492	395	0.85	0.44	1.07	–	[48]
$PrBa_{0.5}Sr_{0.5}Co_2O_{5+\delta}$	1240	981	0.07	–	–	–	[42]
$PrBa_{0.5}Sr_{0.5}CoFeO_{5+\delta}$	–	–	0.11	0.02	–	–	[45]
$PrBa_{0.5}Sr_{0.5}CoFeO_{5+\delta}$	342	260	–	–	–	20.9	[49]
$PrBaCo_{0.5}Fe_{1.5}O_{5+\delta}$	10.2	7.1	–	–	–	19.1	[39]
$PrBaCo_{1.2}Fe_{0.8}O_{5+\delta}$	110	103	1.49	0.29	–	–	[41]
$PrBaCo_{1.4}Fe_{0.6}O_{5+\delta}$	330	303	1.13	0.20	–	–	[41]
$PrBaCo_{1.5}Fe_{0.5}O_{5+\delta}$	132	104	–	–	–	26.0	[39]
$PrBaCo_{1.6}Fe_{0.4}O_{5+\delta}$	404	382	0.50	0.13	–	–	[41]
$PrBaCo_{1.6}Ni_{0.4}O_{5+\delta}$	748	620	–	–	–	16.6	[50]
$PrBaCo_{1.8}Fe_{0.2}O_{5+\delta}$	194	170	1.08	0.20	–	–	[41]
$PrBa_{0.5}Sr_{0.5}Co_{0.5}Fe_{1.5}O_{5+\delta}$	128	95.5	–	–	–	19.2	[49]
$PrBa_{0.5}Sr_{0.5}Co_{1.5}Fe_{0.5}O_{5+\delta}$	–	–	0.06	0.02	–	–	[45]
$PrBa_{0.5}Sr_{0.5}Co_{1.5}Fe_{0.5}O_{5+\delta}$	422	337	–	–	–	21.3	[49]
$PrBa_{0.5}Sr_{0.5}Co_{1.7}Ni_{0.3}O_{5+\delta}$	903	646	13.3	1.75	–	19.7	[51]
$PrBa_{0.5}Sr_{0.5}Co_{1.8}Ni_{0.2}O_{5+\delta}$	835	640	12.4	1.63	–	20.6	[51]
$PrBa_{0.5}Sr_{0.5}Co_{1.9}Ni_{0.1}O_{5+\delta}$	938	771	8.56	1.64	–	21.9	[51]
$PrBaCo_{1.50}Sc_{0.5}O_{5+\delta}$	208	171	0.12	0.03	0.91	19.9	[38]
$PrBaCo_{1.80}Sc_{0.2}O_{5+\delta}$	165	136	0.15	0.03	1.06	22.8	[38]
$PrBaCo_{1.90}Sc_{0.1}O_{5+\delta}$	101	84.4	0.15	0.04	1.07	23.0	[38]
$Pr_{1.05}Ba_{0.95}Co_2O_{5+\delta}$	847	700	–	0.32	–	21.6	[37]
$Pr_{1.10}Ba_{0.90}Co_2O_{5+\delta}$	893	736	–	0.13	–	21.8	[37]
$Pr_{1.20}Ba_{0.80}Co_2O_{5+\delta}$	849	710	–	0.23	–	18.8	[37]
$Pr_{1.30}Ba_{0.70}Co_2O_{5+\delta}$	789	676	–	0.30	–	18.4	[37]
$PrBa_{0.25}Sr_{0.75}Co_2O_{5+\delta}$	1824	1625	0.08	–	–	–	[42]
$PrBa_{0.75}Sr_{0.25}Co_2O_{5+\delta}$	1020	813	0.10	–	–	–	[42]
$PrBaCo_{1.95}Sc_{0.05}O_{5+\delta}$	15.8	13.8	0.16	0.04	1.15	23.6	[38]
$PrBaCo_{0.66}Fe_{0.66}Cu_{0.66}O_{5+\delta}$	144	131	–	0.55	–	16.6	[34]

[a] Measured with LSGM electrolytes.
[b] Measured with GDC electrolyte.

with the bar, while the lowest 25% of the values is represented by the line in the bottom part and the highest 25% with line on top of the bars, at each reported temperature, from 500 to 850 °C at 50 °C interval. This representation allows to visualize the spread of conductivity values for each *RE* based perovskite, and underlines the huge difference in conductivity that can be obtained by varying the substitution and stoichiometry of the compounds. In addition, it's easy to visualize that yttrium based perovskites present conductivity values in average lower than 100 S cm^{-1}. This conductivity is actually considered a threshold value for a successful application as cathode materials according to Steele [82].

A similar graph is reported in Fig. 1B for the ASR values. Most authors report ASR values measured in the temperature range 600–800 °C, and some only report a few values measured at 700 or 750 °C. An indicative values range of ASR in order to consider a material suitable for cathodic application is between 0.10 and 0.20 Ω·cm^2 reported by Steele at al [82]. It must be noted that only few compositions fulfill this condition in the intermediate temperature range (600 °C). The number of compounds that satisfy this requirement of course increases at higher temperatures (700–750 °C), especially in Pr-based compounds.

The wide spread of results is related to both the processes of synthesis and measurement. Unfortunately, slight variations of few percent in the compositions can lead to significant changes in the electric and electrochemical performance. In fact, a slight change in composition and/or lattice parameters strongly affects the

Table 4
Composition, synthetic route, sintering temperature, lattice type and parameters and oxygen content of Pr-based double perovskite cathodes.

Composition	Synthesis method	Sintering temp [°C]	Lattice type	*a* [Å]	*b*[Å]	*c*[Å]	Oxygen content[5+δ]	Reference
$PrBaCo_2O_{5+\delta}$	SS	1100	–	–	–	–	5.68	[18]
$PrBaCo_2O_{5+\delta}$	C	950	O	3.868	3.871	7.576	5.79	[39]
$PrBaCo_2O_{5+\delta}$	P	1100	O	3.915	3.902	7.699	5.78	[42]
$PrBaCo_2O_{5+\delta}$	SG	1150	O	3.896	3.890	7.612	5.77	[29]
$PrBaCo_2O_{5+\delta}$	SG	1000	T	3.909	–	7.638	5.64	[37]
$PrBaCo_2O_{5+\delta}$	SG	950	T	3.894	–	7.636	–	[41]
$PrBaCo_2O_{5+\delta}$	SS	1100	T	3.946	–	7.610	5.89	[33]
$PrBaCo_2O_{5+\delta}$	SS	1100	T[a]	3.902	3.906	7.631	5.70	[19]
$PrBaCoFeO_{5+\delta}$	SG	950	C	3.899	–	–	–	[41]
$PrBaCoFeO_{5+\delta}$	SG	1150	T	3.918	–	7.657	5.79	[44]
$PrBaFe_2O_{5+\delta}$	SG	950	C	3.947	–	–	–	[41]
$PrBaFe_2O_{5+\delta}$	C	950	O	3.928	3.934	7.794	5.88	[39]
$PrSrCo_2O_{5+\delta}$	P	1100	O	5.437	5.403	7.642	6.00	[42]
$PrBaCo_{1.0}Fe_{1.0}O_{5+\delta}$	C	950	O	3.893	3.898	7.681	5.82	[39]
$Pr_{0.3}Y_{0.7}BaCo_2O_{5+\delta}$	SS	1000	T	–	–	–	5.29	[36]
$Pr_{0.5}Y_{0.5}BaCo_2O_{5+\delta}$	SS	1000	T	–	–	–	5.42	[36]
$Pr_{0.7}Y_{0.3}BaCo_2O_{5+\delta}$	SS	1000	T	–	–	–	5.49	[36]
$PrBa_{0.5}Sr_{0.5}Co_2O_{5+\delta}$	P	1100	T	3.869	–	7.732	5.84	[42]
$PrBa_{0.5}Sr_{0.5}Co_2O_{5+\delta}$	SS	1000	T	3.855	–	7.729	5.50	[48]
$PrBa_{0.5}Sr_{0.5}CoFeO_{5+\delta}$	SG	1000	O	3.865	3.864	7.727	5.76	[49]
$PrBaCo_{0.5}Fe_{1.5}O_{5+\delta}$	C	950	O	3.913	3.917	7.766	5.88	[39]
$PrBaCo_{1.2}Fe_{0.8}O_{5+\delta}$	SG	950	C	3.895	–	–	–	[41]
$PrBaCo_{1.4}Fe_{0.6}O_{5+\delta}$	SG	950	C	3.882	–	–	–	[41]
$PrBaCo_{1.5}Fe_{0.5}O_{5+\delta}$	C	950	O	3.875	3.879	7.611	5.81	[39]
$PrBaCo_{1.6}Fe_{0.4}O_{5+\delta}$	SG	950	C	3.879	–	–	–	[41]
$PrBaCo_{1.6}Ni_{0.4}O_{5+\delta}$	SG	1200	T	3.908	–	7.638	–	[50]
$PrBaCo_{1.8}Fe_{0.2}O_{5+\delta}$	SG	950	T	3.889	–	7.661	–	[41]
$PrBa_{0.5}Sr_{0.5}Co_{0.5}Fe_{1.5}O_{5+\delta}$	SG	1000	O	3.883	3.884	7.765	5.82	[49]
$PrBa_{0.5}Sr_{0.5}Co_{1.5}Fe_{0.5}O_{5+\delta}$	SG	1000	O	3.851	3.854	7.715	5.67	[49]
$PrBa_{0.5}Sr_{0.5}Co_{1.7}Ni_{0.3}O_{5+\delta}$	SG	1100	O	3.884	3.860	7.672	–	[51]
$PrBa_{0.5}Sr_{0.5}Co_{1.8}Ni_{0.2}O_{5+\delta}$	SG	1100	O	3.908	3.859	7.612	–	[51]
$PrBa_{0.5}Sr_{0.5}Co_{1.9}Ni_{0.1}O_{5+\delta}$	SG	1100	O	3.863	3.852	7.707	–	[51]
$PrBaCo_{1.50}Sc_{0.5}O_{5+\delta}$	SG	1050	C	–	–	–	5.64	[38]
$PrBaCo_{1.80}Sc_{0.2}O_{5+\delta}$	SG	1050	T	–	–	–	5.71	[38]
$PrBaCo_{1.90}Sc_{0.1}O_{5+\delta}$	SG	1050	T	–	–	–	5.72	[38]
$Pr_{1.05}Ba_{0.95}Co_2O_{5+\delta}$	SG	1000	T	3.899	–	7.632	5.65	[37]
$Pr_{1.10}Ba_{0.90}Co_2O_{5+\delta}$	SG	1000	T	3.891	–	7.619	5.70	[37]
$Pr_{1.20}Ba_{0.80}Co_2O_{5+\delta}$	SG	1000	T	3.878	–	7.620	5.77	[37]
$Pr_{1.30}Ba_{0.70}Co_2O_{5+\delta}$	SG	1000	T	3.870	–	7.624	5.83	[37]
$PrBa_{0.25}Sr_{0.75}Co_2O_{5+\delta}$	P	1100	T	3.842	–	7.677	5.90	[42]
$PrBa_{0.75}Sr_{0.25}Co_2O_{5+\delta}$	P	1100	O	3.897	3.879	7.682	5.79	[42]
$PrBaCo_{1.95}Sc_{0.05}O_{5+\delta}$	SG	1050	T	–	–	–	5.74	[38]
$PrBaCo_{0.66}Fe_{0.66}Cu_{0.66}O_{5+\delta}$	SG	950	T	3.904	–	7.651	–	[34]

[a] Tetragonal with orthorhombic superstructure.

properties of the solid compound [63,83–88].

An even higher irregularity was observed when analyzing ASR values retrieved in literature: a deviation of up to two orders of magnitude can be found in similar materials. This can be explained by the numerous chemical, physical and microstructural parameters actually affecting the results of impedance spectroscopy measurements.

3.3. Electrochemical performance

An optimization of the composition of double perovskites is required in order to reach the best tradeoff between electrochemical performance and cell durability. The electrochemical performance of IT-SOFC cathodes is commonly assessed by measurement of two electrochemical parameters: ASR and electrical conductivity. The ASR value includes material data about the electrons and ions transfer processes occurring at the current collector–electrode–electrolyte interfaces, and about non-charge transfer processes including oxygen surface exchange, solid-state diffusion, and gas-phase diffusion inside and outside the electrode [89]. Therefore both chemical and microstructural parameters can affect ASR.

In order to measure the ASR value, cathodic materials need to be deposited on a pellet made by typical electrolyte materials for IT-SOFC. Thus, the choice of the electrolyte material, the pellet, the layer thickness and adhesion impact on the overall resistance measured. It has been demonstrated also that the choice of the electrolyte material influences the impedance spectroscopy measurements of the same cathode. This result has been explained by some authors in terms of different contact of the cathode layer to the electrolyte support [46]. In addition, even the preparation of the cell assembly influences the final ASR value. In fact, same powders can be deposited using different techniques, with different grains sizes, porosity and layer adhesion, resulting in changes in diffusion paths, number of active sites, connectivity between grains and other elements [5]. The ASR is always monotonically decreasing with increasing the temperature, due to the effect of reduction kinetics and diffusion limitations. The slope of ASR is related to the activation energy of the whole process that brings from O_2 in the gas phase to O^{2-} in the electrolyte, despite the number of possible intermediate steps, and follows an Arrhenius law.

Only a detailed kinetic analysis allows quantifying the influence of different phenomena on the oxygen reduction reaction, therefore understanding the real cathode activity of the materials; nonetheless, this kind of analysis is often time-consuming, and sometimes it is not easy to isolate the different contribution in the

Table 5
Composition, electrical conductivity σ, ASR, activation energy and TEC of Nd-based double perovskite cathodes.

Composition	σ @ 600 °C [S·cm^{-1}]	σ @ 700 °C [S·cm^{-1}]	ASR @ 600 °C [Ω·cm^2]	ASR @ 700 °C [Ω·cm^2]	E act. [eV]	TEC [10^6 K^{-1}]	Reference
$NdBaCo_2O_{5+\delta}$	–	–	0.58	0.11	1.19	22.3	[52]
$NdBaCo_2O_{5+\delta}$	–	–	–	–	–	23.1	[53]
$NdBaCo_2O_{5+\delta}$	952	740	–	–	–	19.1	[20]
$NdBaCo_2O_{5+\delta}$	–	–	–	–	–	23.1	[54]
$NdBaCo_2O_{5+\delta}$	–	–	5.59	0.30	–	–	[26]
$NdBaCo_2O_{5+\delta}$	192	168	0.28	0.04	–	–	[29]
$NdBaCo_2O_{5+\delta}$	–	–	4.52	1.18	–	–	[40]
$NdBaCo_2O_{5+\delta}$	448	343	0.18	0.04	–	–	[55]
$NdBaCo_2O_{5+\delta}$	776	633	1.93	0.70	1.68	21.5	[56]
$NdBaCoCuO_{5+\delta}$	95.1	99.2	1.51	0.28	–	16.9	[57]
$NdBaCoFeO_{5+\delta}$	116	96.8	–	–	–	19.5	[44]
$NdBaCoFeO_{5+\delta}$	70.6	59.2	–	–	–	19.5	[44]
$NdBaCoFeO_{5+\delta}$	102	85.6	2.48	0.90	1.71	20.0	[56]
$NdBaFe_2O_{5+\delta}$	11.7	9.5	–	–	1.08	18.3	[56]
$NdSrCo_2O_{5+\delta}$	2420	2169	0.27	0.05	–	–	[55]
$NdBa_{0.5}Sr_{0.5}Co_2O_{5+\delta}$	–	–	1.17	0.25	1.34	24.3	[52]
$NdBa_{0.5}Sr_{0.5}Co_2O_{5+\delta}$	2412	2100	0.11	–	–	20.3	[58]
$NdBa_{0.5}Sr_{0.5}Co_2O_{5+\delta}$	255	204	1.06	0.55	1.34	–	[48]
$NdBa_{0.5}Sr_{0.5}CoCuO_{5+\delta}$	261	227	3.77	0.52	–	18.9	[57]
$NdBaCo_{0.5}Fe_{1.5}O_{5+\delta}$	39.2	31.2	3.66	1.23	1.80	20.7	[56]
$NdBaCo_{1.5}Fe_{0.5}O_{5+\delta}$	473	392	1.32	0.54	1.45	20.8	[56]
$NdBaCo_{1.6}Ni_{0.4}O_{5+\delta}$	654	521	–	–	1.22	19.4	[50]
$NdBa_{0.5}Sr_{0.5}Co_{1.5}Mn_{0.5}O_{5+\delta}$	717	665	0.16	–	–	14.3	[58]
$NdBa_{0.25}Sr_{0.75}Co_2O_{5+\delta}$	2082	1546	0.13	0.03	1.32	–	[55]
$NdBa_{0.25}Sr_{0.75}CoCuO_{5+\delta}$	211	185	1.25	0.21	–	17.0	[57]
$NdBa_{0.50}Sr_{0.50}Co_2O_{5+\delta}$	1501	1102	0.12	0.03	–	–	[55]
$NdBa_{0.75}Sr_{0.25}Co_2O_{5+\delta}$	550	461	0.17	0.03	–	–	[55]
$NdBa_{0.75}Sr_{0.25}CoCuO_{5+\delta}$	143	123	1.68	0.33	–	18.5	[57]
$NdBa_{0.5}Sr_{0.5}Co_{1.75}Mn_{0.25}O_{5+\delta}$	1133	1004	0.13	–	–	16.4	[58]
$NdBaCo_{0.66}Fe_{0.66}Cu_{0.66}O_{5+\delta}$	91.8	88.0	1.14[a] 0.60[b]	0.21[a] 0.08[b]	–	–	[59]

[a] Measured with GDC electrolyte.
[b] Measured with LSGM electrolyte.

Table 6
Composition, synthetic route, sintering temperature, lattice type and parameters and oxygen content of Nd-based double perovskite cathodes.

Composition	Synthesis method	Sintering temp [°C]	Lattice type	a [Å]	b[Å]	c[Å]	Oxygen content[5+δ]	Reference
$NdBaCo_2O_{5+\delta}$	SS	1100	T	3.903	–	7.614	5.73	[53]
$NdBaCo_2O_{5+\delta}$	SS	1100	T	3.939	–	7.576	5.85	[33]
$NdBaCo_2O_{5+\delta}$	SS	1100	T	3.895	–	7.611	5.78	[20]
$NdBaCo_2O_{5+\delta}$	SS	1100	T	3.903	–	7.614	5.73	[54]
$NdBaCo_2O_{5+\delta}$	SS	1100	T[a]	3.897	3.902	7.612	5.70	[19]
$NdBaCo_2O_{5+\delta}$	SS	1100	–	–	–	–	5.62	[18]
$NdBaCo_2O_{5+\delta}$	SG	1150	O	3.872	3.889	7.599	5.69	[29]
$NdBaCo_2O_{5+\delta}$	P	1100	O	3.918	3.909	7.635	5.78	[55]
$NdBaCo_2O_{5+\delta}$	SS	1100	T	3.896	–	7.619	5.85	[56]
$NdBaCoCuO_{5+\delta}$	SS	1000	T	3.920	–	7.683	5.78	[57]
$NdBaCoFeO_{5+\delta}$	SG	1150	T	3.909	–	7.625	5.67	[44]
$NdBaCoFeO_{5+\delta}$	SS	1100	T	3.912	–	7.704	6.00	[56]
$NdBaFe_2O_{5+\delta}$	SS	1100	C	3.930	–	–	6.00	[56]
$NdSrCo_2O_{5+\delta}$	P	1100	O	5.374	5.420	7.602	6.00	[55]
$NdBa_{0.5}Sr_{0.5}Co_2O_{5+\delta}$	P	1000	T	3.894	–	7.615	5.88	[58]
$NdBa_{0.5}Sr_{0.5}Co_2O_{5+\delta}$	SS	1000	T	3.849	–	7.725	5.23	[48]
$NdBa_{0.5}Sr_{0.5}CoCuO_{5+\delta}$	SS	1000	T	3.871	–	7.664	5.79	[57]
$NdBaCo_{0.5}Fe_{1.5}O_{5+\delta}$	SS	1100	C	3.912	–	–	6.00	[56]
$NdBaCo_{1.5}Fe_{0.5}O_{5+\delta}$	SS	1100	T	3.905	–	7.661	6.00	[56]
$NdBaCo_{1.6}Ni_{0.4}O_{5+\delta}$	SG	1200	T	3.902	–	7.620	–	[50]
$NdBa_{0.5}Sr_{0.5}Co_{1.5}Mn_{0.5}O_{5+\delta}$	P	1000	T	3.856	–	7.705	5.83	[58]
$NdBa_{0.25}Sr_{0.75}Co_2O_{5+\delta}$	P	1100	T	3.895	–	7.610	5.89	[55]
$NdBa_{0.25}Sr_{0.75}CoCuO_{5+\delta}$	SS	1000	T	3.894	–	7.667	5.69	[57]
$NdBa_{0.50}Sr_{0.50}Co_2O_{5+\delta}$	P	1100	T	3.894	–	7.615	5.89	[55]
$NdBa_{0.75}Sr_{0.25}Co_2O_{5+\delta}$	P	1100	O	3.896	3.883	7.646	5.78	[55]
$NdBa_{0.75}Sr_{0.25}CoCuO_{5+\delta}$	SS	1000	T	3.900	–	7.672	5.75	[57]
$NdBa_{0.5}Sr_{0.5}Co_{1.75}Mn_{0.25}O_{5+\delta}$	P	1000	T	3.858	–	7.713	5.78	[58]
$NdBaCo_{0.66}Fe_{0.66}Cu_{0.66}O_{5+\delta}$	SG	1400	T	3.923	–	7.696	5.44	[59]
$NdBaCo_{0.66}Fe_{0.66}Cu_{0.66}O_{5+\delta}$	SG	1400	T	3.923	–	7.696	5.44	[59]

[a] Tetragonal with orthorhombic superstructure.

Table 7
Composition, electrical conductivity σ, ASR, activation energy and TEC of Sm-based double perovskite cathodes.

Composition	σ @ 600 °C [S·cm^{-1}]	σ @ 700 °C [S·cm^{-1}]	ASR @ 600 °C [Ω·cm^2]	ASR @ 700 °C [Ω·cm^2]	E act. [eV]	TEC [10^6 K^{-1}]	Reference
$SmBaCo_2O_{5+\delta}$	–	–	–	–	–	21.2	[53]
$SmBaCo_2O_{5+\delta}$	836	633	–	–	–	17.1	[20]
$SmBaCo_2O_{5+\delta}$	556	443	0.19	–	–	–	[61]
$SmBaCo_2O_{5+\delta}$	–	–	–	–	–	20.8	[54]
$SmBaCo_2O_{5+\delta}$	–	–	16.5	1.53	–	–	[26]
$SmBaCo_2O_{5+\delta}$	226	193	0.54	0.09	–	–	[29]
$SmBaCo_2O_{5+\delta}$	749	627	–	–	–	21.1	[62]
$SmBaCo_2O_{5+\delta}$	–	–	–	1.60	–	–	[40]
$SmBaCo_2O_{5+\delta}$	–	–	0.52	0.10	1.23	–	[63]
$SmSrCo_2O_{5+\delta}$	2137	1585	0.28	–	–	–	[61]
$SmSrCo_2O_{5+\delta}$	615	502	–	0.07	–	22.7	[64]
$SmSrCoMnO_{5+\delta}$	39.5	45.9	–	–	–	13.8	[64]
$SmBa_{0.5}Sr_{0.5}Co_2O_{5+\delta}$	–	–	0.74	0.35	–	–	[65]
$SmBa_{0.5}Sr_{0.5}Co_2O_{5+\delta}$	–	–	0.81	0.35	1.07	–	[47]
$SmBaCo_{1.4}Fe_{0.6}O_{5+\delta}$	275	230	–	–	–	21.2	[62]
$SmBaCo_{1.6}Fe_{0.4}O_{5+\delta}$	342	283	–	–	–	20.8	[62]
$SmBaCo_{1.6}Ni_{0.4}O_{5+\delta}$	413	329	–	–	–	20.6	[50]
$SmBaCo_{1.8}Fe_{0.2}O_{5+\delta}$	483	395	–	–	–	20.4	[62]
$SmSrCo_{1.2}Mn_{0.8}O_{5+\delta}$	70.5	76.0	–	0.14	1.29	17.4	[64]
$SmSrCo_{1.4}Mn_{0.6}O_{5+\delta}$	118	110	–	0.11	1.02	18.1	[64]
$SmSrCo_{1.6}Mn_{0.4}O_{5+\delta}$	203	173	–	0.09	1.28	20.7	[64]
$SmSrCo_{1.8}Mn_{0.2}O_{5+\delta}$	358	296	–	0.08	1.19	21.3	[64]
$SmBa_{0.5}Sr_{0.5}Co_{1.5}Fe_{0.5}O_{5+\delta}$	261	245	32.2	6.31	–	–	[66]
$Sm_{0.92}BaCo_2O_{5+\delta}$	576	472	–	–	–	–	[63]
$Sm_{0.95}BaCo_2O_{5+\delta}$	503	411	0.32	0.07	1.06	–	[63]
$Sm_{0.97}BaCo_2O_{5+\delta}$	371	302	0.32	0.07	1.07	–	[63]
$SmBa_{0.25}Sr_{0.75}Co_2O_{5+\delta}$	1373	1049	0.14	–	–	–	[61]
$SmBa_{0.50}Sr_{0.50}Co_2O_{5+\delta}$	1006	787	0.14	–	–	–	[61]
$SmBa_{0.75}Sr_{0.25}Co_2O_{5+\delta}$	741	577	0.17	–	–	–	[61]

Table 8
Composition, synthetic route, sintering temperature, lattice type and parameters and oxygen content of Sm-based double perovskite cathodes.

Composition	Synthesis method	Sintering temp [°C]	Lattice type	a [Å]	b[Å]	c[Å]	Oxygen content[5+δ]	Reference
$SmBaCo_2O_{5+\delta}$	SS	1100	O	3.886	7.833	7.560	5.60	[53]
$SmBaCo_2O_{5+\delta}$	SS	1100	T	3.928	–	7.540	5.69	[33]
$SmBaCo_2O_{5+\delta}$	SS	1100	O	3.880	3.907	7.559	5.65	[20]
$SmBaCo_2O_{5+\delta}$	P	1100	O	3.900	3.918	7.591	5.62	[61]
$SmBaCo_2O_{5+\delta}$	SS	1100	O	3.886	7.833	7.560	5.61	[54]
$SmBaCo_2O_{5+\delta}$	SS	1100	T[a]	3.886	3.909	7.566	5.40	[19]
$SmBaCo_2O_{5+\delta}$	SS	1100	–	–	–	–	5.54	[18]
$SmBaCo_2O_{5+\delta}$	SG	1150	O	3.866	3.885	7.569	5.68	[29]
$SmBaCo_2O_{5+\delta}$	C	1100	O	3.889	7.839	7.563	5.61	[62]
$SmBaCo_2O_{5+\delta}$	SG	1150	O	3.898	3.887	7.561	5.46	[63]
$SmSrCo_2O_{5+\delta}$	P	1150	O	5.403	5.383	7.626	6.00	[61]
$SmBaCo_{1.4}Fe_{0.6}O_{5+\delta}$	C	1100	T	3.904	–	7.618	5.76	[62]
$SmBaCo_{1.6}Fe_{0.4}O_{5+\delta}$	C	1100	O	3.888	7.826	7.599	5.74	[62]
$SmBaCo_{1.6}Ni_{0.4}O_{5+\delta}$	SG	1200	O	3.916	3.887	7.577	–	[50]
$SmBaCo_{1.8}Fe_{0.2}O_{5+\delta}$	C	1100	O	3.888	7.828	7.579	5.71	[62]
$SmBa_{0.5}Sr_{0.5}Co_{1.5}Fe_{0.5}O_{5+\delta}$	SG	1200	T	3.865	–	7.610	–	[66]
$Sm_{0.95}BaCo_2O_{5+\delta}$	SG	1150	O	3.902	3.889	7.569	5.37	[63]
$Sm_{0.97}BaCo_2O_{5+\delta}$	SG	1150	O	3.902	3.888	7.567	5.36	[63]
$SmBa_{0.25}Sr_{0.75}Co_2O_{5+\delta}$	P	1150	T	3.834	–	7.664	5.87	[61]
$SmBa_{0.50}Sr_{0.50}Co_2O_{5+\delta}$	P	1150	T	3.867	–	7.586	5.76	[61]
$SmBa_{0.75}Sr_{0.25}Co_2O_{5+\delta}$	P	1150	O	3.886	3.891	7.589	5.70	[61]

[a] Tetragonal with orthorhombic superstructure.

impedance spectra. A comparison between the complete evaluation and discussion of spectroscopy contributions would be of great importance, in order to figure out how much of the electrical resistance is affected by macroscopic properties and how much is the actual material contribute. However, since only few papers [24,30,58,65,79,86,90–94] present this accurate analysis, it's still challenging to compare the results, either to reach a helpful conclusion.

However, the conductivity helps to evaluate the electric efficiency of the materials. The reported total conductivity (σ_T) is composed of two contributes: electronic (σ_e) and ionic (σ_i) conductivities. In order to make a cathodic material satisfying, both conductivities have to be as high as possible. In almost every paper classified, only the global value of conductivity is reported, without subdivision in its two contributes. However, ionic conductivity in these materials is usually at least two orders of magnitude lower than electronic conductivity, hence the measured value is usually attributed to electronic charge carriers [95].

Double perovskite materials can present a variety of conduction behaviors, in terms of temperature dependency of the global conductivity. If the conductivity increases with temperature, the material owns a semiconductor-like behavior, while metallic-like conductivity decreases with increasing temperature. Frequently, double perovskites exhibit both these conductivity mechanisms; a

Table 9
Composition, electrical conductivity σ, ASR, activation energy and TEC of Gd-based double perovskite cathodes.

Composition	σ @ 600 °C [S·cm^{-1}]	σ @ 700 °C [S·cm^{-1}]	ASR @ 600 °C [Ω·cm^2]	ASR @ 700 °C [Ω·cm^2]	E act. [eV]	TEC [10^6 K^{-1}]	Reference
$GdBaCo_2O_{5+\delta}$	483	377	–	–	–	16.6	[67]
$GdBaCo_2O_{5+\delta}$	–	–	–	–	–	20.1	[53]
$GdBaCo_2O_{5+\delta}$	–	–	1.73	–	1.34	–	[68]
$GdBaCo_2O_{5+\delta}$	–	–	3.10	–	–	–	[68]
$GdBaCo_2O_{5+\delta}$	–	–	1.35	–	1.27	–	[68]
$GdBaCo_2O_{5+\delta}$	375	359	2.11	0.34	1.21	18.1	[36]
$GdBaCo_2O_{5+\delta}$	–	–	1.08	0.12	1.43	–	[69]
$GdBaCo_2O_{5+\delta}$	512	406	–	–	–	16.6	[20]
$GdBaCo_2O_{5+\delta}$	231[a]	198[a]	0.42[a]	0.04[a]	–	–	[27]
	210[b]	179[b]	0.18[b]	0.01[b]			
$GdBaCo_2O_{5+\delta}$	–	–	–	–	–	18.4	[70]
$GdBaCo_2O_{5+\delta}$	–	–	21.7	5.77	–	–	[26]
$GdBaCo_2O_{5+\delta}$	105	89.9	0.25	0.03	–	–	[29]
$GdBaCo_2O_{5+\delta}$	–	–	2.44	0.40	–	–	[40]
$GdBaCo_2O_{5+\delta}$	–	–	0.40	0.08	–	20.8	[71]
$GdBaCo_2O_{5+\delta}$	–	–	1.14	0.43	–	19.9	[72]
$GdBaCo_2O_{5+\delta}$	484	378	2.54	0.87	1.75	19.9	[56]
$GdBaCoCuO_{5+\delta}$	50.8	68.3	4.78	0.65	–	–	[57]
$GdBaCoCuO_{5+\delta}$	–	–	2.48	0.68	–	13.9	[72]
$GdBaCoFeO_{5+\delta}$	73.6	70.9	3.38	1.09	1.86	18.8	[56]
$GdSrCo_2O_{5+\delta}$	1155	934	–	–	1.29	18.8	[67]
$GdBa_{0.4}Sr_{0.6}Co_2O_{5+\delta}$	1111	932	–	–	–	19.5	[67]
$GdBa_{0.5}Sr_{0.5}Co_2O_{5+\delta}$	–	–	1.11	0.55	1.22	–	[47]
$GdBa_{0.5}Sr_{0.5}Co_2O_{5+\delta}$	2178	2031	–	–	–	–	[73]
$GdBa_{0.5}Sr_{0.5}Co_2O_{5+\delta}$	640	521	0.13	–	–	–	[74]
$GdBa_{0.5}Sr_{0.5}CoCuO_{5+\delta}$	64.1	66.2	7.21	0.84	–	–	[57]
$GdBa_{0.5}Sr_{0.5}CoFeO_{5+\delta}$	66.6	56.9	–	–	–	–	[73]
$GdBa_{0.5}Sr_{0.5}CoFeO_{5+\delta}$	27.5	25.0	0.08	–	–	–	[74]
$GdBa_{0.6}Sr_{0.4}Co_2O_{5+\delta}$	1023	821	–	–	–	18.3	[67]
$GdBa_{0.8}Sr_{0.2}Co_2O_{5+\delta}$	804	664	–	–	–	18.0	[67]
$GdBaCo_{1.5}Fe_{0.5}O_{5+\delta}$	274	229	1.21	0.56	1.20	19.6	[56]
$GdBaCo_{1.7}Ni_{0.3}O_{5+\delta}$	–	–	0.55	0.15	–	15.5	[71]
$GdBaCo_{1.8}Ni_{0.2}O_{5+\delta}$	–	–	0.48	0.14	–	17.1	[71]
$GdBaCo_{1.9}Ni_{0.1}O_{5+\delta}$	–	–	0.44	0.12	–	18.9	[71]
$GdBaCuCo_{0.5}Fe_{0.5}O_{5+\delta}$	7.5	9.9	–	1.40	–	14.4	[75]
$GdBa_{0.5}Sr_{0.5}Co_{0.5}Fe_{1.5}O_{5+\delta}$	8.3	8.8	–	–	–	–	[73]
$GdBa_{0.5}Sr_{0.5}Co_{1.5}Fe_{0.5}O_{5+\delta}$	694	620	2.33	0.96	–	21.8	[73]
$GdBa_{0.5}Sr_{0.5}Co_{1.5}Fe_{0.5}O_{5+\delta}$	261	225	0.10	–	–	–	[74]
$GdBa_{0.25}Sr_{0.75}CoCuO_{5+\delta}$	30.7	37.3	6.11	0.80	1.05	–	[57]
$GdBa_{0.75}Sr_{0.25}CoCuO_{5+\delta}$	39.5	47.6	6.11	0.80	–	–	[57]
$GdBaCo_{0.66}Fe_{0.66}Cu_{0.66}O_{5+\delta}$	–	–	1.56	0.46	–	14.6	[72]
$GdBaCo_{0.66}Fe_{0.66}Ni_{0.66}O_{5+\delta}$	–	–	1.91	0.54	–	17.5	[72]

[a] Sample annealed in air.
[b] Sample annealed in Ar.

change in the conductivity mechanism is often observed as a function of temperature: generally, a transition from semiconductor (at low temperature) to metallic-like behavior (at high temperature) is reported, and it follows that these materials exhibit a maximum in the conductivity values at intermediate temperatures. The onset temperature of this transition changes depending on the chemical composition, but it's usually situated between 300 and 600 °C. The change in the slope of the conductivity vs temperature curve is ascribed to the loss of oxygen occurring in the lattice when increasing the temperature, which is in turn triggered by the reduction of Co^{4+} ($Co^{\bullet}_{Co}$) to Co^{3+} (Co^{x}_{Co}); the defect reaction that occurs can be represented using Kröger-Vink notation [96]:

$$2Co^{\bullet}_{Co} + O^{x}_{O} \leftrightarrow 2Co^{x}_{Co} + v^{\bullet\bullet}_{O} + \frac{1}{2}O_2 \quad (1)$$

In order to maintain charge neutrality, for each oxygen vacancy ($v^{\bullet\bullet}_{O}$) generated in the lattice during the heating process the loss of two p-type carriers ($Co^{\bullet}_{Co}$) is needed, resulting in a conductivity decrease [76].

3.4. Chemical compatibility with electrolytes

The chemical compatibility among the cell components is an important requirement for the choice of IT-SOFC materials; an investigation of reactivity of cathode materials with the common electrolytes is therefore mandatory in order to determine an optimal electrode-electrolyte couple. Even if IT-SOFCs are meant to operate at lower temperature, the inter-diffusion of cations at the interface could promote the formation of new phases either in the fabrication step or during the cell operation, possibly leading to the formation of an insulating layer at the interface that would obstruct the ionic and electronic transport. Many of the interesting double perovskite materials for cathodic application have been characterized also in this respect.

The most common approach to investigate chemical compatibility is by heating up a physical mixture of cathode and electrolyte powders at high temperature for several hours, then analyzing the occurrence of new phases or inter-diffusion by means of X-Ray Diffraction (XRD). This easy and common procedure demonstrates if the cathode material is compatible with selected electrolyte. By the way, a negative result should be reported as a clear evidence of incompatibility, but a positive one is limited to the analysis condition. Moreover, sometimes no clear evidence of new phase formation or cation inter-diffusion can be assessed based only on XRD measurements. In the investigated literature the chemical compatibility is usually checked by applying relatively mild

Table 10
Composition, synthetic route, sintering temperature, lattice type and parameters and oxygen content of Gd-based double perovskite cathodes.

Composition	Synthesis method	Sintering temp [°C]	Lattice type	*a* [Å]	*b*[Å]	*c*[Å]	Oxygen content[5+δ]	Reference
$GdBaCo_2O_{5+\delta}$	SS	1000	O	3.876	3.912	7.541	5.61	[67]
$GdBaCo_2O_{5+\delta}$	SS	1100	O	3.875	7.822	7.533	5.53	[53]
$GdBaCo_2O_{5+\delta}$	SS	1000	O	–	–	–	5.48	[36]
$GdBaCo_2O_{5+\delta}$	SS	1100	O	3.873	3.912	7.529	5.57	[20]
$GdBaCo_2O_{5+\delta}$	SS	1200	T	–	–	–	5.30	[27]
$GdBaCo_2O_{5+\delta}$	SS	1200	O	–	–	–	5.80	[27]
$GdBaCo_2O_{5+\delta}$	SS	1200	T	–	–	–	5.40	[27]
$GdBaCo_2O_{5+\delta}$	SS	1100	T[a]	3.875	3.911	7.534	5.40	[19]
$GdBaCo_2O_{5+\delta}$	SS	1100	–	–	–	–	5.42	[18]
$GdBaCo_2O_{5+\delta}$	SG	1150	O	3.860	3.861	7.519	5.66	[29]
$GdBaCo_2O_{5+\delta}$	SS	1100	O	3.877	7.825	7.542	5.57	[56]
$GdBaCoCuO_{5+\delta}$	SS	1000	T	3.894	–	7.604	5.64	[57]
$GdBaCoFeO_{5+\delta}$	SS	1100	T	3.903	–	7.643	6.00	[56]
$GdSrCo_2O_{5+\delta}$	SS	1000	O	5.373	5.402	7.572	6.00	[67]
$GdBa_{0.4}Sr_{0.6}Co_2O_{5+\delta}$	SS	1000	T	3.840	–	7.549	5.83	[67]
$GdBa_{0.5}Sr_{0.5}Co_2O_{5+\delta}$	P	1100	T	3.862	–	7.558	–	[74]
$GdBa_{0.5}Sr_{0.5}CoCuO_{5+\delta}$	SS	1000	T	3.866	–	7.576	5.66	[57]
$GdBa_{0.5}Sr_{0.5}CoFeO_{5+\delta}$	P	1150	T	3.871	–	7.637	–	[74]
$GdBa_{0.6}Sr_{0.4}Co_2O_{5+\delta}$	SS	1000	T	3.856	–	7.546	5.79	[67]
$GdBa_{0.8}Sr_{0.2}Co_2O_{5+\delta}$	SS	1000	T	3.872	–	7.550	5.69	[67]
$GdBaCo_{1.5}Fe_{0.5}O_{5+\delta}$	SS	1100	T	3.895	–	7.592	5.98	[56]
$GdBa_{0.5}Sr_{0.5}Co_{1.5}Fe_{0.5}O_{5+\delta}$	P	1150	T	3.869	–	7.594	–	[74]
$GdBa_{0.25}Sr_{0.75}CoCuO_{5+\delta}$	SS	1000	T	3.880	–	7.593	5.58	[57]
$GdBa_{0.75}Sr_{0.25}CoCuO_{5+\delta}$	SS	1000	T	3.880	–	7.596	5.68	[57]
$GdBaCo_{0.66}Fe_{0.66}Cu_{0.66}O_{5+\delta}$	SG	1000	T	3.885	–	7.635	–	[72]

[a] Tetragonal with orthorhombic superstructure.

Table 11
Composition, electrical conductivity σ, ASR, activation energy and TEC of Y-based double perovskite cathodes.

Composition	σ @ 600 °C [S·cm^{-1}]	σ @ 700 °C [S·cm^{-1}]	ASR @ 600 °C [Ω·cm^2]	ASR @ 700 °C [Ω·cm^2]	E act. [eV]	TEC [10^6 K^{-1}]	Reference
$YBaCo_2O_{5+\delta}$	189	160	–	0.11	0.49	16.3	[25]
$YBaCo_2O_{5+\delta}$	23.6	21.2	0.53	0.13	0.92	–	[30]
$YBaCo_2O_{5+\delta}$	135	121	3.93	1.03	–	–	[66]
$YBaCo_2O_{5+\delta}$	–	–	–	–	–	13.8	[53]
$YBaCo_2O_{5+\delta}$	69.8	58.5	–	0.09	–	17.8	[24]
$YBaCo_2O_{5+\delta}$	119	120	0.99	0.21	–	–	[76]
$YBaCo_2O_{5+\delta}$	215	178	–	–	–	–	[77]
$YBaCo_2O_{5+\delta}$	153	122	–	–	–	15.8	[20]
$YBaCo_2O_{5+\delta}$	–	–	–	–	–	19.1	[23]
$YBaCo_2O_{5+\delta}$	24.9	–	–	–	–	–	[78]
$YBaCo_2O_{5+\delta}$	37.8	31.7	4.59	0.63	–	–	[29]
$YSrCo_2O_{5+\delta}$	–	–	1.37	0.41	0.97	–	[23]
$YBa_{0.2}Sr_{0.8}Co_2O_{5+\delta}$	–	–	1.34	0.22	1.50	–	[23]
$YBa_{0.3}Sr_{0.7}Co_2O_{5+\delta}$	–	–	1.08	0.17	1.50	–	[23]
$YBa_{0.4}Sr_{0.6}Co_2O_{5+\delta}$	–	–	1.55	0.24	1.50	19.8	[23]
$YBa_{0.5}Sr_{0.5}Co_2O_{5+\delta}$	424	337	–	–	–	18.8	[25]
$YBa_{0.5}Sr_{0.5}Co_2O_{5+\delta}$	371	291	1.78	0.36	1.21	–	[76]
$YBa_{0.5}Sr_{0.5}Co_2O_{5+\delta}$	70.3	59.4	–	–	–	–	[78]
$YBa_{0.6}Sr_{0.4}Co_2O_{5+\delta}$	318	283	2.24	0.35	–	–	[76]
$YBa_{0.7}Sr_{0.3}Co_2O_{5+\delta}$	512	450	3.29	0.57	–	–	[76]
$YBa_{0.8}Sr_{0.2}Co_2O_{5+\delta}$	445	396	1.07	0.20	–	–	[76]
$YBa_{0.9}Sr_{0.1}Co_2O_{5+\delta}$	165	145	2.04	0.46	–	–	[76]
$YBaCo_{1.2}Cu_{0.8}O_{5+\delta}$	27.9	38.3	–	0.18	–	13.4	[24]
$YBaCo_{1.2}Fe_{0.8}O_{5+\delta}$	23.3	20.7	–	–	–	–	[77]
$YBaCo_{1.4}Cu_{0.6}O_{5+\delta}$	39.8	47.4	–	0.12	–	14.7	[24]
$YBaCo_{1.4}Fe_{0.6}O_{5+\delta}$	27.1	22.6	–	–	–	–	[25]
$YBaCo_{1.4}Fe_{0.6}O_{5+\delta}$	44.1	36.4	–	–	–	–	[77]
$YBaCo_{1.6}Cu_{0.4}O_{5+\delta}$	55.4	57.8	–	0.18	–	15.7	[24]
$YBaCo_{1.6}Fe_{0.4}O_{5+\delta}$	55.9	47.1	–	0.15	0.53	18.0	[25]
$YBaCo_{1.6}Fe_{0.4}O_{5+\delta}$	64.7	53.4	–	–	–	–	[77]
$YBaCo_{1.8}Cu_{0.2}O_{5+\delta}$	67.1	71.6	–	0.15	–	16.7	[24]
$YBaCo_{1.8}Fe_{0.2}O_{5+\delta}$	128	107	–	0.13	0.52	17.3	[25]
$YBaCo_{1.8}Fe_{0.2}O_{5+\delta}$	136	112	–	–	–	–	[77]
$YBa_{0.5}Sr_{0.5}Co_{1.4}Cu_{0.6}O_{5+\delta}$	114	106	–	0.18	1.18	16.4	[79]

calcination processes (in the temperature range of 900–1100 °C for 6–12 h) and sometimes even for very short times and low temperatures, suggesting that slightly higher temperatures or longer times would have shown some evidence of reactivity. A more severe characterization of the reactivity is therefore suggested for a meaningful understanding of the long-term reactivity. In fact, when long-lasting stability tests are performed, the measured ASR values increase over time due to (at least) some microstructural

Table 12
Composition, synthetic route, sintering temperature, lattice type and parameters and oxygen content of Y-based double perovskite cathodes.

Composition	Synthesis method	Sintering temp [°C]	Lattice type	*a* [Å]	*b*[Å]	*c*[Å]	Oxygen content[5+δ]	Reference
$YBaCo_2O_{5+\delta}$	SS	1100	T	3.879	–	7.509	–	[25]
$YBaCo_2O_{5+\delta}$	SG	1050	T	3.874	–	7.502	–	[66]
$YBaCo_2O_{5+\delta}$	SS	1100	T	11.616	–	7.493	5.51	[53]
$YBaCo_2O_{5+\delta}$	SG	1000	T	11.627	–	7.509	–	[24]
$YBaCo_2O_{5+\delta}$	SS	1100	T	11.615	–	7.496	–	[77]
$YBaCo_2O_{5+\delta}$	SS	1100	T	3.874	–	7.483	5.41	[20]
$YBaCo_2O_{5+\delta}$	SS	1125	T	3.878	–	7.498	5.31	[23]
$YBaCo_2O_{5+\delta}$	SG	1150	O	3.846	3.954	7.485	5.41	[29]
$YBa_{0.3}Sr_{0.7}Co_2O_{5+\delta}$	SS	1125	T	–	–	–	5.54	[23]
$YBa_{0.4}Sr_{0.6}Co_2O_{5+\delta}$	SS	1125	T	–	–	–	5.50	[23]
$YBa_{0.5}Sr_{0.5}Co_2O_{5+\delta}$	SS	1125	–	–	–	–	5.40	[23]
$YBaCo_{1.2}Cu_{0.8}O_{5+\delta}$	SG	1000	T	11.658	–	7.551	–	[24]
$YBaCo_{1.2}Fe_{0.8}O_{5+\delta}$	SS	1100	T	11.632	–	7.566	–	[77]
$YBaCo_{1.4}Cu_{0.6}O_{5+\delta}$	SG	1000	T	11.658	–	7.546	–	[24]
$YBaCo_{1.4}Fe_{0.6}O_{5+\delta}$	SS	1100	T	3.893	–	7.555	–	[25]
$YBaCo_{1.4}Fe_{0.6}O_{5+\delta}$	SS	1100	T	11.637	–	7.554	–	[77]
$YBaCo_{1.6}Cu_{0.4}O_{5+\delta}$	SG	1000	T	11.656	–	7.541	–	[24]
$YBaCo_{1.6}Fe_{0.4}O_{5+\delta}$	SS	1100	T	3.885	–	7.535	–	[25]
$YBaCo_{1.6}Fe_{0.4}O_{5+\delta}$	SS	1100	T	11.636	–	7.532	–	[77]
$YBaCo_{1.8}Cu_{0.2}O_{5+\delta}$	SG	1000	T	11.648	–	7.534	–	[24]
$YBaCo_{1.8}Fe_{0.2}O_{5+\delta}$	SS	1100	T	3.881	–	7.519	–	[25]
$YBaCo_{1.8}Fe_{0.2}O_{5+\delta}$	SS	1100	T	11.623	–	7.529	–	[77]

Table 13
Composition, synthetic route, sintering temperature, lattice type and parameters and oxygen content of Dy, Eu, Ho and Tb based double perovskite cathodes.

Composition	Synthesis method	Sintering temp [°C]	Lattice type	*a*[Å]	*b*[Å]	*c*[Å]	Oxygen content[5+δ]	Reference
$DyBaCo_2O_{5+\delta}$	SS	1100	T	3.879	–	7.505	–	[53]
$DyBaCo_2O_{5+\delta}$	SS	1100	T	3.876	3.879	7.504	5.30	[19]
$DyBaCo_2O_{5+\delta}$	SS	1100	–	–	–	–	5.36	[18]
$EuBaCo_2O_{5+\delta}$	SS	1100	O	3.882	7.828	7.546	5.56	[53]
$EuBaCo_2O_{5+\delta}$	SS	1100	T	3.883	3.916	7.541	5.40	[19]
$EuBaCo_2O_{5+\delta}$	SS	1100	–	–	–	–	5.52	[18]
$HoBaCo_2O_{5+\delta}$	SS	1100	T	3.873	–	7.495	–	[53]
$HoBaCo_2O_{5+\delta}$	SS	1125	T	3.882	–	7.488	5.14	[23]
$HoBaCo_2O_{5+\delta}$	SS	1100	T	3.873	3.872	7.496	5.30	[19]
$HoBaCo_2O_{5+\delta}$	SS	1100	–	–	–	–	5.25	[18]
$TbBaCo_2O_{5+\delta}$	SS	1100	O	3.868	7.818	7.518	–	[53]
$TbBaCo_2O_{5+\delta}$	SS	1100	T	3.867	3.908	7.516	5.40	[19]
$TbBaCo_2O_{5+\delta}$	SS	1100	–	–	–	–	5.41	[18]

Table 14
Effective ionic radii rare earths (12-fold coordination, from Refs. [80];* 9-fold coordination, from Ref. [81]).

Rare earth ion	Effective ionic radius
Y^{3+}	1.075*
La^{3+}	1.36
Pr^{3+}	1.32
Nd^{3+}	1.31
Sm^{3+}	1.28
Gd^{3+}	1.27
Eu^{3+}	1.28
Dy^{3+}	1.24
Ho^{3+}	1.23
Tb^{3+}	1.25

rearrangements at the cathode–electrolyte interface [97,98].

Among commercially available electrolyte materials, YSZ has been reported to react with several double perovskites materials, such as the $PrBaCo_{2-x}Fe_xO_{5+\delta}$ series [39] where the authors reported reactivity for temperatures as low as 700 °C for 20 h with the appearance of small peaks belonging to $PrCoO_3$ or $PrFeO_3$ phases, while at 900 °C a larger amount of $BaZrO_3$ develops; in $SmBaCo_{2-x}Fe_xO_{5+\delta}$ series [62], the growth of $BaZrO_3$ is identified after annealing at 900 °C for 24 h that is not influenced by the amount of iron in the structure. Tarancon et al. [99] proposed a complete characterization for $GdBaCo_2O_{5+\delta}$ double perovskite stability, concluding that it presents high reactivity with YSZ even at low temperature (700 °C). However, YSZ isn't commonly considered as promising electrolyte for intermediate temperature range unless it is used in very thin layers, therefore few data are available about its reactivity with double perovskite compounds. LSGM and doped ceria electrolytes (GDC, SDC) instead, show higher ionic conductivity in the intermediate temperature range and are better suited for low-temperature operation [5]. Zhou et al. [100], published their results about the chemical compatibility of $REBaCo_2O_{5+\delta}$ (RE = Pr, Nd, Sm and Gd) compounds with samarium doped ceria (SDC) and LSGM, reporting that neither additional peaks nor structural changes were detected after 5 h at 1000 °C. Several other works instead, report reaction issues for compatibility tests performed in more harsh conditions, especially for LSGM as electrolyte: Tarancon et al. [99] investigated the stability of $GdBaCo_2O_{5+\delta}$ also with GDC and LSGM and found the formation of a small amount of secondary phase with both electrolyte materials after annealing at 1000 °C. Moreover, the secondary phase content increases at higher temperature, ending up at 1200 °C with a solid solution between $GdBaCo_2O_{5+\delta}$ and LSGM with a mixed cubic perovskite lattice; this result is ascribed to the similar lattice structures between the two compounds. It is generally understood that the more the lattices are similar between cathode and electrolyte, the easier is the occurrence of interface reaction. Therefore

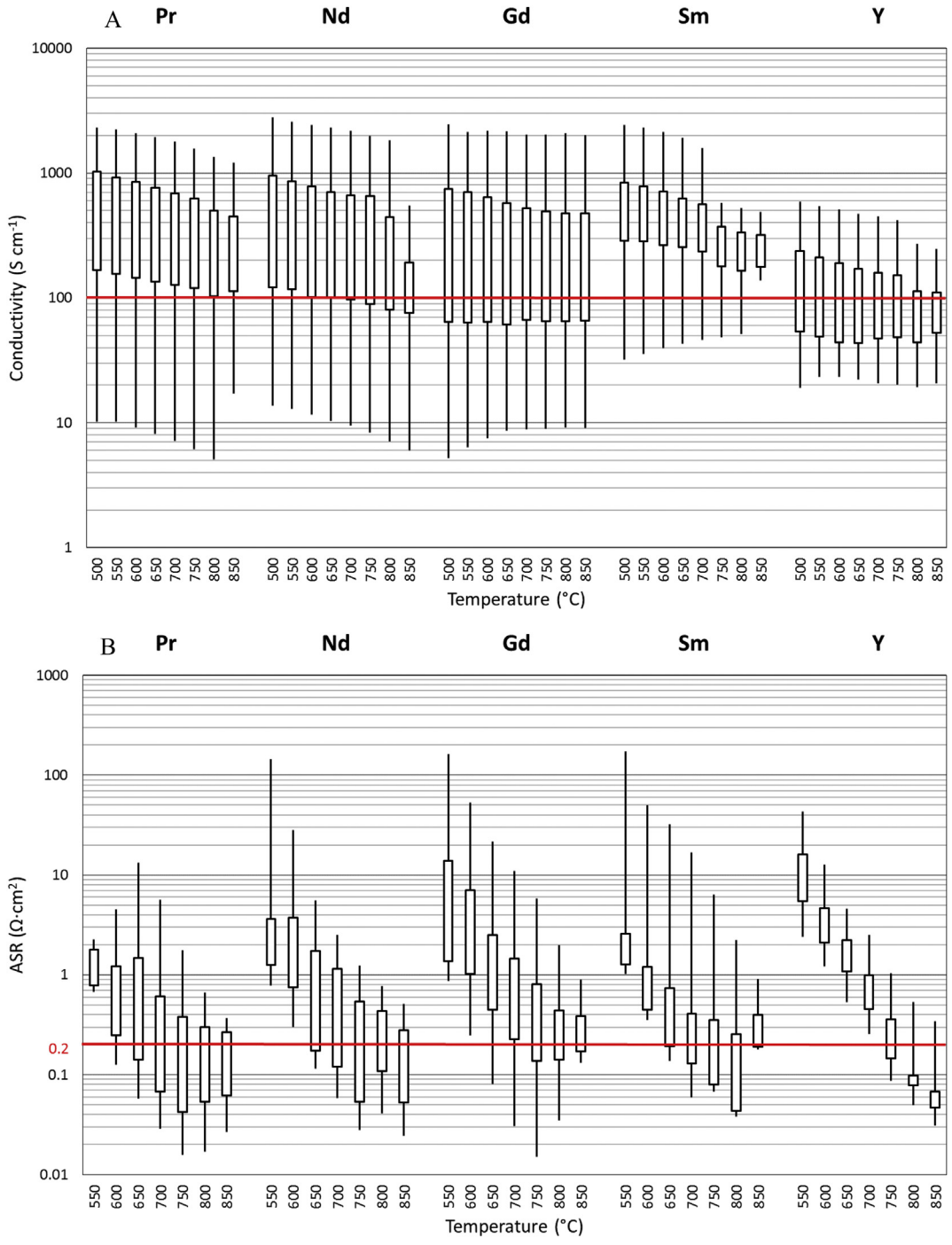

Fig. 1. Total electric conductivities (σ [S·cm^{-1}], panel A) and ASRs [Ω·cm^2], panel B) of the investigated compounds grouped by A site rare earth, reported split in quartiles.

it is expected that double perovskite materials could present more reactivity issues with LSGM than with GDC or SDC doped ceria electrolytes ($A_{1-x}A'_xO_2$) that adopt a fluorite structure.

The doping effect on chemical stability is different based on material properties: Y-based double perovskites usually present a phase instability when undoped, while it has been demonstrated that the substitution of Ba with Sr enhance not only the chemical stability, but also the chemical compatibility with GDC electrolyte [23,67]. In addition, a proper amount of Sr substitution into the double perovskite composition could reduce the ion inter-diffusion issue with LSGM electrolyte, because it could reduce the sharp concentration gradient of Sr at the cathode–electrolyte interface. However, sometimes the presence of a dopant element can worsen the electrolyte-electrode compatibility. Jin et al. [59] for example reported the formation of a secondary phase, $SmCu_2O_4$, at the interface between SDC and $NdBaCo_{0.66}Fe_{0.66}Cu_{0.66}O_{5+\delta}$ after calcination at 950 °C for 10 h in air, while the same compound was found to be inert with GDC and LSGM at the same annealing conditions.

3.5. Thermal expansion mismatch

In order to extend the cell durability it is important to have similar TEC values between the cathode and the electrolyte

materials. A thermal mismatch as small as possible is required to reduce the strain occurring at the interface during the thermal cycles of the cell. Co based double perovskites usually present a much higher TEC value than typical electrolytes ($10.4–12.3 \cdot 10^6\ K^{-1}$ for LSGM [101] and $11.4–12.7 \cdot 10^6\ K^{-1}$ for rare earths doped ceria [102]). High TECs in double perovskites are related to Co^{3+} cation state that, at high temperature, can pass from low spin (LS, $t^6_{2g}e^0_g$) to intermediate (IS, $t^5_{2g}e^1_g$) and to high spin (HS, $t^4_{2g}e^2_g$), progressively increasing its ionic radius [103]. Hence, to reduce TEC in these materials Co is partially or completely substituted with different metals (especially Fe), that can mitigate these disadvantages. In addition, typical dopants cost is often much lower than that of cobalt, possibly reducing the global development cost of a Co based cathode material [25,34,51,56,64,103–105].

Aanother strategy to effectively reduce the problems related to TECs mismatch is by using composite cathodes, which can minimize the undesired thermal expansion discontinuity at the electrolyte–cathode interface without affecting the cathode optimal composition [91]. A brief survey is reported in the next section.

3.6. Composite cathodes

SOFC developers used composite materials to improve the performance of the anode [106]; the first oness were studied with the aim of enhancing the electrochemical properties. In fact, mixtures with different fractions of electrolytic and cathodic materials were investigated, revealing better performance, most likely caused by the increase of the triple phase boundary length [107,108]. This effect has been studied even with mathematical models [109–113]. Subsequently, researchers mainly focused their attention on materials that show both ionic and electronic conduction (MIEC), in order to optimize the tradeoff between electronic conductivity and oxygen reduction kinetics [106]. Nowadays, high performance materials are available, but the high TEC of many of these materials is still an open issue. Instead of reducing TEC values by doping strategies, the use of composite cathodes has been attempted [58]. In addition, composite cathodes also represent a breakthrough for oxygen reduction reaction mechanism; a decrease in ASR is reported when composites with around 50% weight ratio of electrolyte material are tested [65,106,107,114]. Besides, the addition of high amounts of electrolyte compound (i.e. electronic insulators) to cathode material leads to a significant drop in electronic conductivity of the composite; this is often accounted for by the limited continuity of the cathodic phase in the composite [106]. A further advancement in composite cathodes is represented by the so-called graded configuration. Graded cathodes are made by different layers of composite cathodes with an increasing fraction of electrolyte phase, in order to gradually reduce the differences in thermal expansion between cathode and electrolyte. In addition, a functionally graded cathode can show also an enhancement of the overall electrochemical performance due to the opportunity to optimize different parameters in each composite layer [91,100].

4. Review of the most promising materials

Sometimes it is very problematic to compare similar or even identical compounds through different papers, because of the variety of the reported preparation methods and characterizations. However, many publications confirm the positive outcome that McKinlay et al. [78] that reports a marked improvement of the electrical conductivity of these compounds when Sr replaces half of the Ba in $YBa_{1-x}Sr_xCo_2O_{5+\delta}$

Many publications confirm this trend, explaining it as a direct cause of the decrease in oxide-ion vacancy concentration due to an increase of both oxygen content and average Co oxidation state, related to the smaller size of Sr^{2+} ion with respect to Ba^{2+} [42]. Since the oxygen vacancy concentration decreases, the ionic conductivity should decrease too, but the overall conductivity increases due to the higher electronic contribute. In order to increase electronic conductivity, a material needs a large concentration of electronic holes or free electrons, elements controlling the ability of moving electrons inside material lattice. However, producing a material with both high electronic and ionic conductivity is quite challenging; any negative defect introduced in the lattice, such as A site acceptor dopants or deficiency, can be compensated by either the formation of ionic defects (oxide-ion vacancies) or by electronic defects (holes) originated by oxidation of Co^{3+} to Co^{4+} [16]. The distribution of these chemical defects is the main factor determining electrical and electrochemical properties of the double perovskite cathode materials. However, what determines the compensation mechanism by electronic holes or oxygen vacancies, it is not completely known yet.

According to Kim at al. the higher concentration of smaller Co^{4+} ions than Co^{3+} is also related to a relief of the compressive stress in the O–Co–O bonding, that increase toward the ideal value of 180°, causing a structural change from orthorhombic to tetragonal [67]. The tetragonal structure exhibits faster oxygen transport in the bulk and surface and higher catalytic activity for the oxygen reduction reaction as compared to an orthorhombic structure because it provides a more symmetrical structure [55]. Symmetry in cell lattice structure allows a better overlap between 3d orbitales from the transition metal (Co and its dopants) and 2p orbitales from oxygen ions [29,83,88].

Electronic conduction within perovskite-related oxides is believed to occur via electron hopping along $Co^{4+}–O^{2-}–Co^{3+}$ bonds. The exact mechanism is thought to resemble a Zerner double exchange process, which is closely related to both the mobility of the electrical carriers and the path of diffusion [29]. Thus, increasing oxygen vacancies impedes the electron hopping pathway and causes a reduction of electronic conductivity [59].

In addition, the complete substitution of Ba with Sr does not yield the alternate double perovskite structure, due to the comparable ionic radii of rare earths and Sr^{2+}. In fact, also other papers show that $LnSrCo_2O_{5+\delta}$ oxygen content is usually near to 6, demonstrating that these materials prefer to allocate in disordered $Ln_{0.5}Sr_{0.5}CoO_3$ layers, instead of ordered alternated $LnCoO_3$ and $SrCoO_3$ layers [55,67]. When δ increases, oxygen ions fill the Ln-O layer, proving pyramidal CoO_5 structures become octahedral CoO_6, removing lattice charge ordering and reducing crystallographic unit cell along the *b* direction [115]. These simple non-doped perovskites present a very high electrical conductivity due to more symmetric cell structure, usually a cubic one. However, these materials do not provide enough oxygen vacancies, resulting in poor ionic conduction. Although adding acceptor dopants can induce vacancies formation and thus ionic conduction behavior, it also causes instability and very high TEC [5].

However, focusing only on electrical conductivity would be restrictive for the optimization of IT-SOFCs cathodes; maximizing oxygen content leads to very high electronic conductivity but it could decrease the ionic one, depending on the defect chemistry of the compound. Low ionic conductivity reveals lack of oxygen vacancies, which usually has a detrimental effect on the oxygen surface exchange rate, that in turn is likely to cause high polarization resistances (ASR) in cases where the surface exchange process is the rate determining step [86].

The lowest ASR reported in literature has been achieved by Choi at al [45]. for the compound with general formula $PrBa_{0.5}Sr_{0.5}Co_{1.5}Fe_{0.5}O_{5+\delta}$. In this paper is reported a value of 0.056 Ω cm^2 at 600 °C using GDC as electrolyte for the impedance measurements. This publication suggests this material as

promising for cathode applications, but in the same year Jiang at al [49]. presented a paper containing the characterization of the same compound, with less encouraging ASR values. The only measurement reported by Jiang is 0.07 Ω cm^2 at 800 °C, that is even higher than the result reported at 600 °C by Choi [45]. This discrepancy can be partially explained by the adoption of LSGM as electrolyte support in the production of symmetric cells for impedance measurements, but it also reveals the difficulty in comparison between same compounds within two different papers.

After McKinlay et al. [78] and Kim et al. [67] publications, many researches followed their steps, producing double perovskites with general formula $LnBa_{0.5}Sr_{0.5}Co_2O_{5+\delta}$, using different rare earths [46,47,52,65,76,105] or trying also with B site dopants (Cu [57,79,103], Mn [58,64], Ni [51], Fe [45,74]) in order to reduce TEC. However the lowest TEC value has been achieved by Wang et al. that tried to optimize the Mn content in double perovskite $SmSrCo_{2-x}Mn_xO_{5+\delta}$. A value equal to $13.7 \cdot 10^6$ K^{-1} is reported for $SmSrCoMnO_{5+\delta}$, but, although this compound would be suitable for matching with commercial electrolyte TECs, the substitution of half Co leads to a dramatic drop in conductivity from 615 S cm^{-1} for $SmSrCo_2O_{5+\delta}$ to 40 S cm^{-1} at 600 °C. In this material larger Mn^{3+} ions replace smaller Co^{3+} causing a bending of (Co,Mn)–O–(Co,Mn) bonds, decreasing the angle below 180° and consequently resulting in a metal to semiconductor behavior transition [64].

Kim et al. have produced another Mn-doped double perovskite series with the aims of lowering TEC value and optimizing electrochemical performance. TEC value drops from $20.27 \cdot 10^6$ K^{-1} for $NbBa_{0.5}Sr_{0.5}Co_2O_{5+\delta}$ to $14.33 \cdot 10^6$ K^{-1} for $NbBa_{0.5}Sr_{0.5}Co_{1.5}Mn_{0.5}O_{5+\delta}$. Although a significant drop in performance is reported, both conductivity and ASR are still acceptable for IT-SOFC cathode application. At 600 °C the electrical conductivity of $NbBa_{0.5}Sr_{0.5}Co_{1.5}Mn_{0.5}O_{5+\delta}$ is equal to 718 S cm^{-1} and the ASR is 0.156 Ω cm^2. Both parameters are worse than those of the respective Mn-free compound (2410 S cm^{-1} and 0.115 Ω cm^2), but Mn-doped material meets the general requirements for a cathode material, as showed by the obtained power density (1.20 W cm^{-2} at 600 °C) [58].

In order to deeply analyze material performance, compounds have been split into different groups based on A site rare earth element. In next sections a summary of the electrochemical parameters of the most studied compositions (*RE*$BaCo_2O_{5+\delta}$ and *RE*$Ba_{0.5}Sr_{0.5}Co_2O_{5+\delta}$., with *RE* = Pr, Nd, Sm and Gd) will be presented.

4.1. Pr-based double perovskites

Pr-based compounds are the most popular double perovskites present in literature for number of characterizations. Fig. 2A shows the temperature dependence of the conductivity for the most common Pr-based double perovskite: $PrBaCo_2O_{5+\delta}$. It's evident that there's a large mismatch between different results, as conductivity values at 300 °C amount to 200 S cm^{-1} in the compound investigated by Zhang et al. [29] and reach up to 1500 S cm^{-1} in the one prepared by Jiang et al. [37]; similarly, at 800 °C σ changes from 100 S cm^{-1} in Ref. [29] to 600 S cm^{-1} in Ref. [37].

The temperature dependence of ASR reported in different papers using different electrolyte materials is shown in Fig. 2B for $PrBaCo_2O_{5+\delta}$. Even when considering the most promising results, $PrBaCo_2O_{5+\delta}$ presents ASR values not perfectly suited for cathodic application at temperatures below 600 °C. However, it was found that perovskites performance can be enhanced by Sr doping on Ba

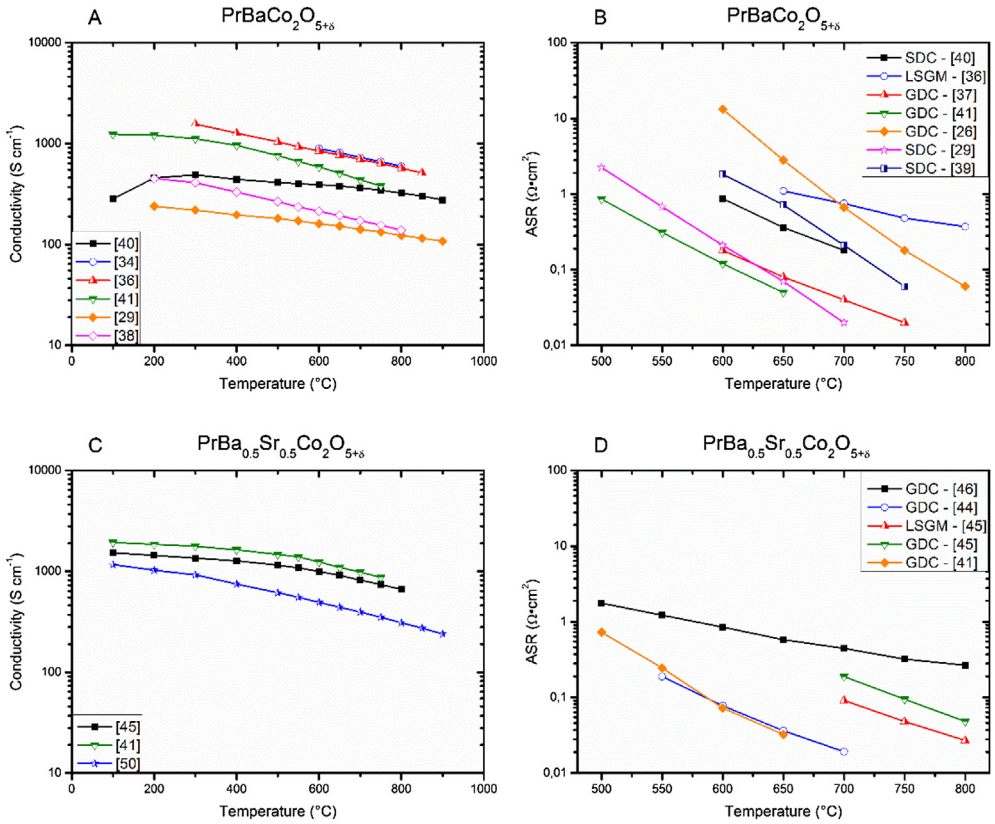

Fig. 2. Electrochemical characteristics of $PrBaCo_2O_{5+\delta}$ – total electrical conductivities σ ([S·cm^{-1}], panel A) and ASR ([Ω•cm^2], panel B) – and of $PrBa_{0.5}Sr_{0.5}Co_2O_{5+\delta}$: total electrical conductivities σ ([S·cm^{-1}], panel C) and ASR ([Ω•cm^2], panel D). The legends report the electrolyte used for the measurement of ASRs.

site [46,42,51]. The typical Sr-doped compound synthesized present half of the barium substituted with strontium ($PrBa_{0.5}Sr_{0.5}Co_2O_{5+\delta}$). The electrochemical parameters and their temperature dependence for this materials are reported in Fig. 2C and D. The enhancement of the conductivity it is noticeable: at 600 °C conductivities are enhanced from the range 150–900 S cm^{-1} without Sr doping up to 600–1400 S cm^{-1} for doped materials. A similar trend is obtained analyzing the ASR that at 600 °C improves from 0.1 to 13 Ω cm^2 to 0.05–1 Ω cm^2.

Considering the ASRs reported in literature, the most promising Pr-based perovskite series are $PrBa_{0.5}Sr_{0.5}Co_{2-x}Fe_xO_{5+\delta}$, synthesized by Choi at al. [45], and $PrBa_{1-x}Sr_xCo_2O_{5+\delta}$, produced by Park at al [42]. Park's compounds also present the highest conductivity values in Pr-based perovskites literature, but is well known that these materials result unsuitable for cathodic application with the common electrolytes, due to their much higher TEC value. Unfortunately Park et al. do not report in their paper any measurement of thermal expansion coefficient of these promising materials, but a large discrepancy with the TEC of similar materials is not expected.

4.2. Nd-based double perovskites

Considering Nd as A site rare earth for perovskites, the number of publications containing electrochemical characterization is slightly lower than those about Pr-based ones. The $NdBaCo_2O_{5+\delta}$ conductivity values at 600 °C range from 200 to 1000 S cm^{-1} (Fig. 3A) while ASR values vary from 0.2 to 6 Ω cm^2 at 600 °C, and by up to two order of magnitudes at 500 °C (Fig. 3B). In Fig. 3C and D are reported the electrochemical parameters of $NdBa_{0.5}Sr_{0.5}Co_2O_{5+\delta}$ perovskites. In analogy with what reported for Pr-based ones, the conductivities and ASRs are much improved from the respective undoped perovskites. In fact, conductivity values are found in the range of 300–2400 S cm^{-1}, while ASR ones between 0.1 and 1.2 Ω cm^2. The best performing Nd-based perovskite materials have been synthesized by Yoo et al. [55] with $NdBa_{1-x}Sr_xCo_2O_{5+\delta}$ perovskite series. These compounds show the lowest ASR values in Nd-based double perovskite literature and some of the highest conductivity ones.

4.3. Gd-based double perovskites

Compounds containing Gd in the A site were investigated in a large number of papers, mainly in the form of the parent $GdBaCo_2O_{5+\delta}$ double perovskite. However, this material seems to be less efficient than previously discussed ones. Conductivity at 600 °C is reported between 100 and 500 S cm^{-1} (Fig. 4A), while ASR (Fig. 4B) ranges from 0.3 to 22 Ω cm^2. A great improvement has been achieved with the substitution of Sr, but only few researchers (Refs. [47,73]) investigated the electrochemical properties of this compound, as can be seen in Fig. 4C and D, reporting conductivity and ASR as a function of temperature.

4.4. Sm-based double perovskites

Sm-based materials are less investigated, but some interesting results were reported. As an example, at 600 °C the measured conductivities range between 250 and 850 S cm^{-1}, while ASR values range from 0.2 to 15 Ω cm^2, as reported in Fig. 5A and B

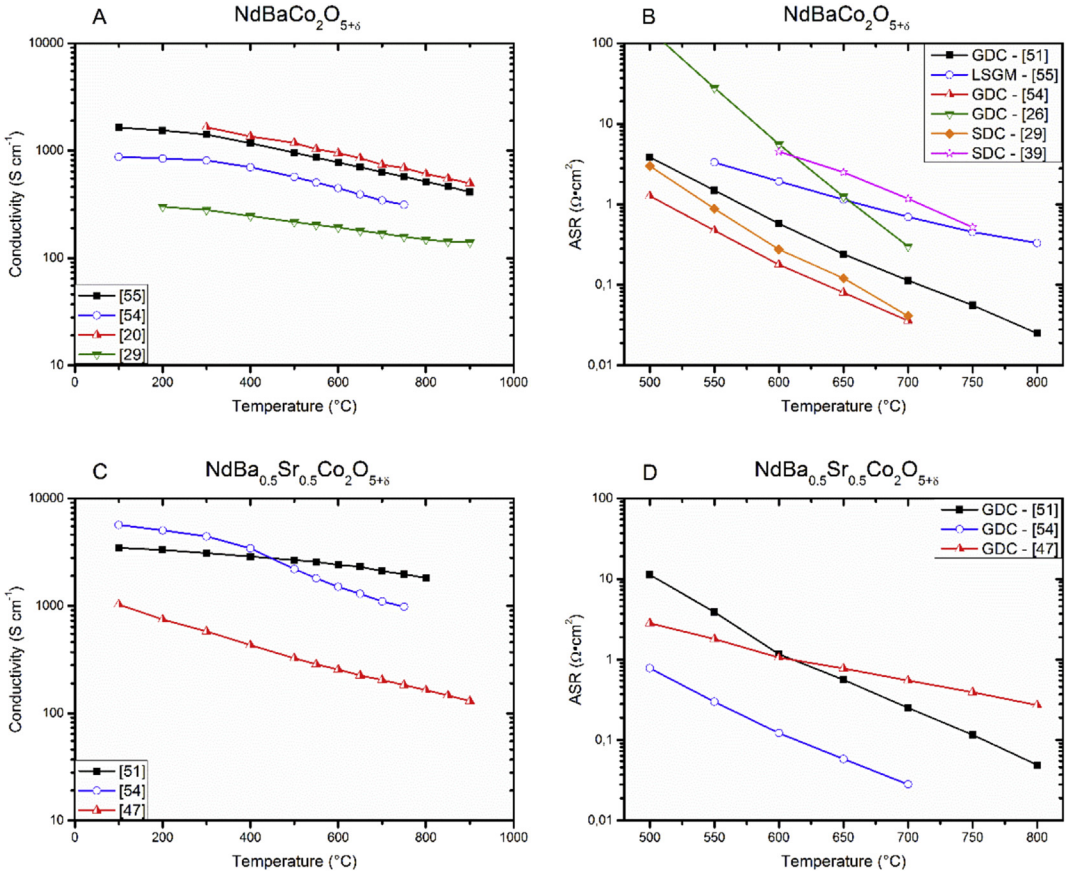

Fig. 3. Electrochemical characteristics of $NdBaCo_2O_{5+\delta}$ – total electrical conductivities σ ([S·cm^{-1}], panel A) and ASR ([Ω•cm^2], panel B) – and of $NdBa_{0.5}Sr_{0.5}Co_2O_{5+\delta}$: total electrical conductivities σ ([S·cm^{-1}], panel C) and ASR ([Ω•cm^2], panel D). The legends report the electrolyte used for the measurement of ASRs.

respectively for $SmBaCo_2O_{5+\delta}$. Only few papers report a characterization of doped double perovskites with Sm, and in Fig. 5C and D the conductivity and ASRs are shown for $SmBa_{0.5}Sr_{0.5}Co_2O_{5+\delta}$ compounds. Comparing number of publications about Sm with Pr or Nd ones, appears clear that the interest of researchers has been focused on the elements presented above, and it appears that some efforts could still devoted to a further improvement of $SmBaCo_2O_{5+\delta}$ derivate compounds.

5. Doping strategies in double perovskites

The effect of doping on double perovskite materials can be different, depending on the site where the substitution takes place and of course on the parent compound; by the way, some similarities between the effects of the same doping strategy on different compounds can be mentioned.

5.1. A site doping

The most common doping is the substitution of Ba in A′ site with Sr. As underlined in the previous sections, Sr doping mainly enhance electrochemical performance of double perovskite material (see Figs. 2–5). Both electrical parameters of interest give a positive feedback for materials series with increasing Sr doping content. As can be inferred by the curves reported in Fig. 6A–D, for almost every compound series, the electrical conductivity increases with increasing Sr concentration, in the whole temperature range. The maximum of conductivity is often reached with complete substitution of Ba with Sr, but at the same time this usually causes a significant worsening in the oxygen reduction reaction kinetics, as revealed by the measured ASRs: Fig. 6E–F shows the dependence of ASR from Sr doping content at different temperatures. The lowest ASR values are found for those compounds with the strontium content $x \geq 0.5$, except for the point with $x = 1$ (i.e. compounds where Ba is completely replaced by Sr) in every series characterized. Indeed at $x = 1$ the ASR sharply increases at any temperature. The main drawback related to Sr doping is the slight increase of TEC values. Unfortunately, most of the authors that investigated Sr-doped double perovskites series do not report any thermal expansion measurement, except for the paper by Kim et al. [67]. Table 15 reports TEC values of $GdBa_{1-x}Sr_xCo_2O_{5+\delta}$ compounds ($0.0 < x < 1.0$) in the 80–900 °C temperature range. However, even the lowest TEC value reported for the SR-doped materials ($16.6 \cdot 10^6\ K^{-1}$ [67]) is still far from matching the TECs of commercial electrolytes ($12–14 \cdot 10^6\ K^{-1}$, GDC, SDC and LSGM). In addition, Gd-based compounds present the lowest average TEC values among all rare earths. In fact, considering only double perovskites with Gd as rare earth in A site, the average TEC value present in literature is $17.9 \cdot 10^6\ K^{-1}$.

For what regards the compounds bearing other elements in A site, average TEC increases for Y, Nd, Sm and Pr, presenting respectively 18.8, 19.6, 19.7 and $20.6 \cdot 10^6\ K^{-1}$.

5.2. B site doping

5.2.1. Iron doping

A common doping element used to replace Co in B site is Fe. This substitution is realized with the purpose of reducing TEC values in

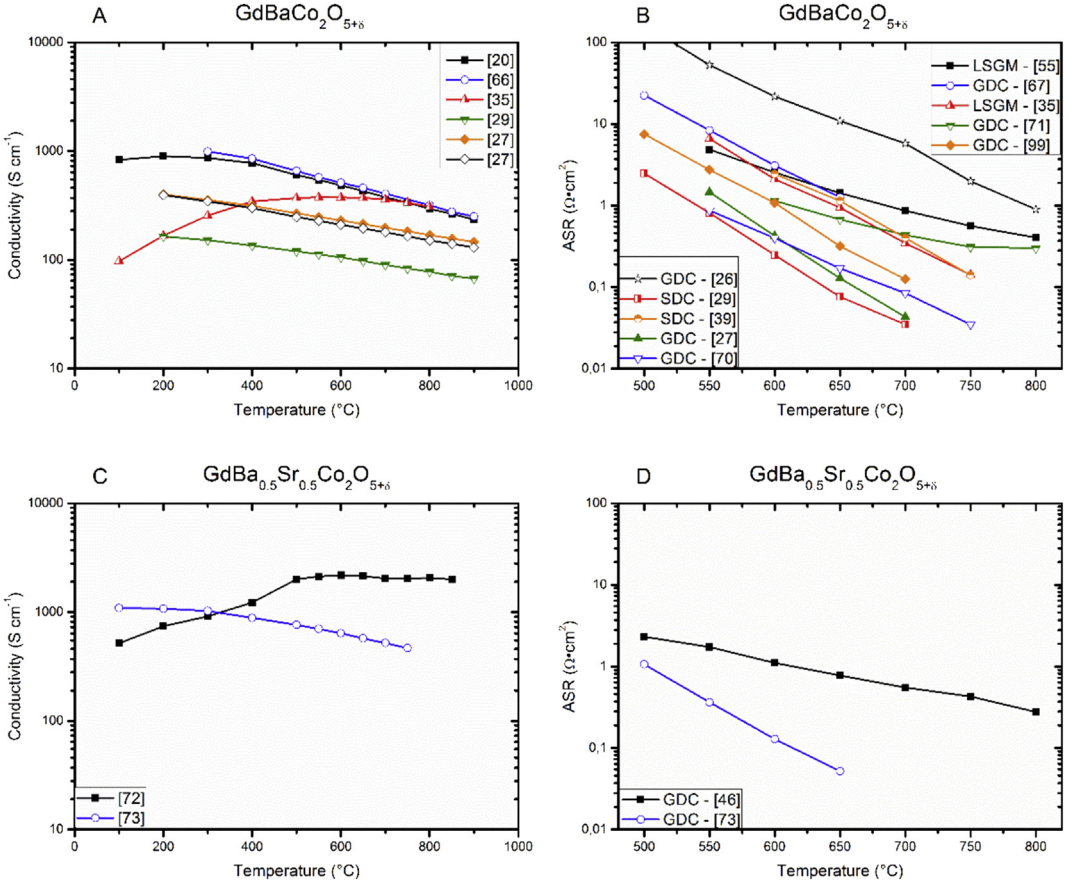

Fig. 4. Electrochemical characteristics of $GdBaCo_2O_{5+\delta}$ – total electrical conductivities σ ([$S \cdot cm^{-1}$], panel A) and ASR ([$\Omega \cdot cm^2$], panel B) – and of $GdBa_{0.5}Sr_{0.5}Co_2O_{5+\delta}$: total electrical conductivities σ ([$S \cdot cm^{-1}$], panel C) and ASR ([$\Omega \cdot cm^2$], panel D). The legends report the electrolyte used for the measurement of ASRs.

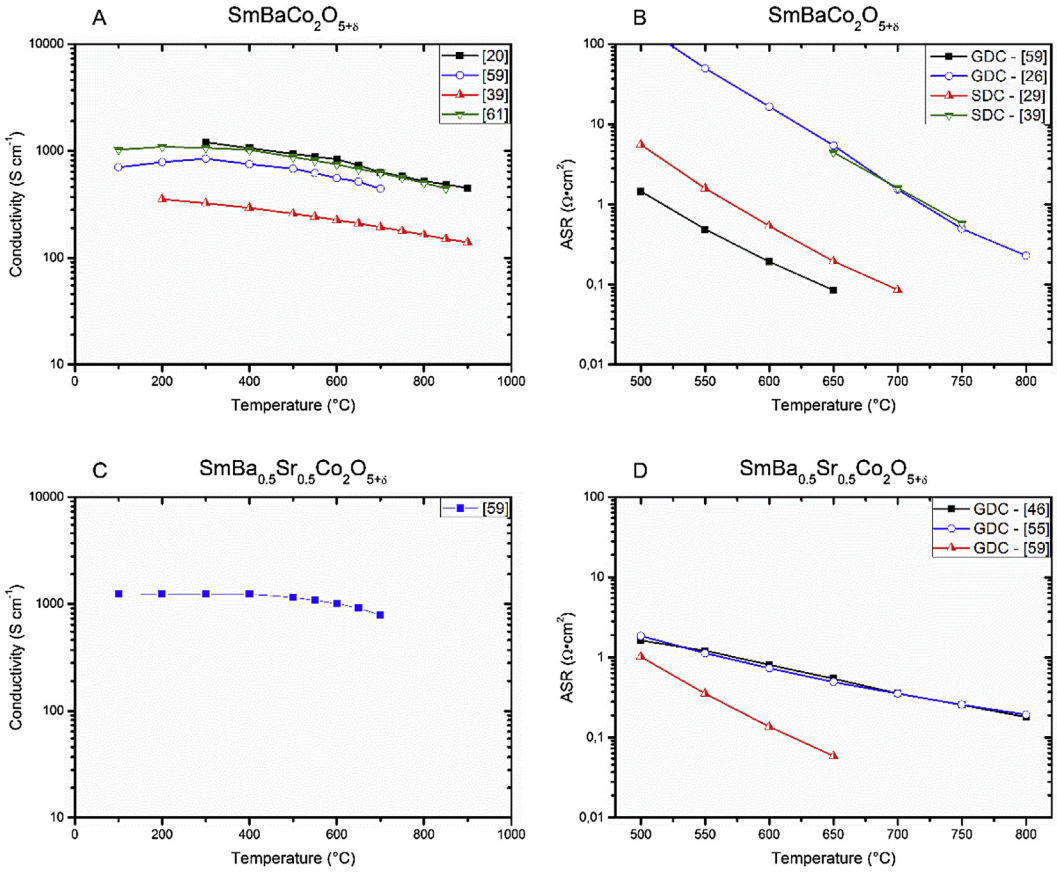

Fig. 5. Electrochemical characteristics of $SmBaCo_2O_{5+\delta}$ – total electrical conductivities σ ([S·cm^{-1}], panel A) and ASR ([Ω•cm^2], panel B) – and of $SmBa_{0.5}Sr_{0.5}Co_2O_{5+\delta}$: total electrical conductivities σ ([S·cm^{-1}], panel C) and ASR ([Ω•cm^2], panel D). The legends report the electrolyte used for the measurement of ASRs.

Co based double perovskite materials, since Fe produces stronger bonds with oxygen compared to Co [56].

Many publications report a series of double perovskites with increasing Fe doping for cathodic application, mostly resulting in a worsening of the electrochemical performance, but also a reduction of TEC value. However, according to the available data *RE*$BaCo_{2-y}Fe_yO_{5+\delta}$ compounds do not satisfy the TEC requirement for cathodic application with common electrolytes yet, since the TEC decease by Fe content is too feeble. Kim et al. [56] presented a publication containing the thermic characterization of $NdBaCo_{2-y}Fe_yO_{5+\delta}$ (with y = 0, 0.5, 1, 1.5, 2) and $GdBaCo_{2-y}Fe_yO_{5+\delta}$ (with y = 0, 0.5, 1) series, obtaining a decrease of TEC values respectively from 21.5 to $18.3\cdot10^6$ K^{-1} and from 19.9 to $18.8\cdot10^6$ K^{-1}. Zhao et al. [39] achieved a better TEC reduction on $PrBaCo_{2-y}Fe_yO_{5+\delta}$ (with y = 0, 0.5, 1, 1.5, 2) series, reporting a maximum TEC value for y = 0.5 compound, equal to 26 10^6 K^{-1} and a minimum of 17.2 10^6 K^{-1}, for the compound with y = 2. However, these slight TEC reductions do not balance out the significant drop in electrochemical performance related to the replacement of Co with Fe. As is shown in Fig. 7A–D, conductivity decrease monotonically with Fe content for almost every series reported. The only exception is represented by $PrBaCo_{2-y}Fe_yO_{5+\delta}$ obtained by Zou et al. [41] that increases its electrical conductivity at y = 0.4 to y = 0.6 iron content. Thou, those samples undergo a structural change from tetragonal to cubic at y > 0.4. This variation of structure leads to a more symmetrical lattice cell, hence a consequent increase in electrical conductivity. Of particular interest is that the dependence of ASR from Fe content (Fig. 7E–H) presents the minimum value for the same composition $PrBaCo_{1.6}Fe_{0.4}O_{5+\delta}$. Zou et al. [41] are the only authors reporting such a detailed characterization of Fe doped double perovskites in the full stoichiometry range between 0 and 1. However, other two Fe-doped series [56] seem to confirm the positive decrease of ASR for the compounds with 0.5 Fe content, but do not present neither the cubic transition nor the conductivity improvement. Anyway the Nd-based series proposed by Kim at el [56]. present the structure transition from tetragonal to cubic for y ≥ 1.5 comppositions. Another investigation of Fe substitution on B site of Pr-based double perovskite is proposed by Yoo et al. [116]. In this paper the oxygen fluxes have been measured through membranes made by $PrBaCo_{2-y}Fe_yO_{5+\delta}$ (with y = 0, 0.2, 0.5, 1, 1.5, 2), resulting in an overall decrease of the specific oxygen flux with Fe content. In this paper, the transition from tetragonal to cubic structure is reported only for the perovskite with y = 1 and y = 1.5 as Fe content.

Also the influence of other elements have been investigated as B site dopants, especially transition metals such as Ni [50,51,71,117], Cu [24,118] and Mn [58]. Moreover, some authors reported also a Sc substituted compound [38].

5.2.2. Ni doping

One of the most common element used to dope double perovskites on B site is Ni. In literature characterizations about double perovskites doped with Ni are present for several rare earths on A site. Although B site doping is mainly made to achieve a reduction of TEC values, the electrochemical performance cannot be ignored. In fact, Ni doping leads to considerable improvements of thermal expansion behavior but, regarding conductivity and ASR, high doping levels cause a drop in the electrochemical performance.

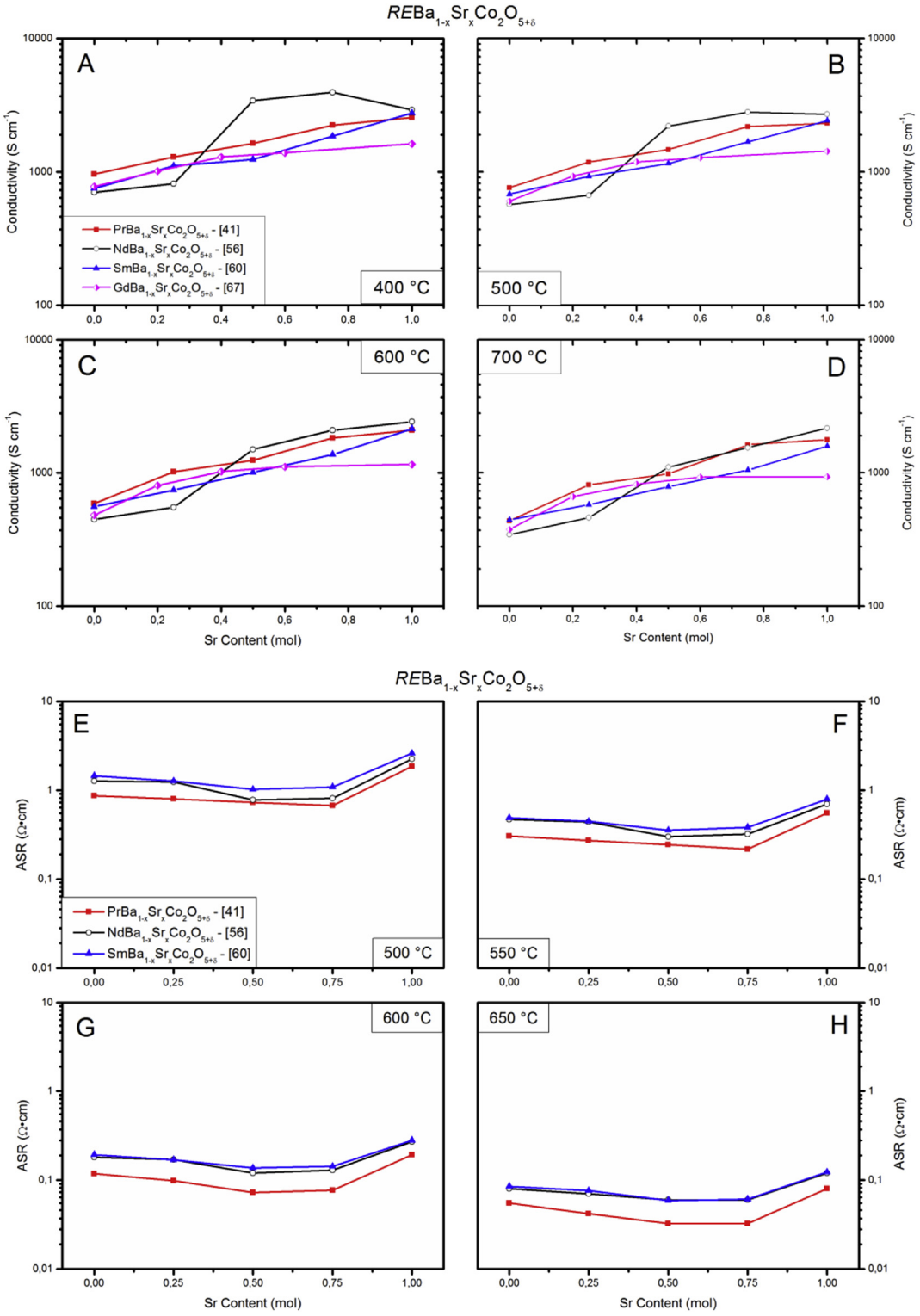

Fig. 6. Electrochemical characteristics of selected $REBa_{1-x}Sr_xCo_2O_{5+\delta}$ compounds as a function of strontium content x: total electrical conductivities σ ([$S \cdot cm^{-1}$], 400 °C, panel A; 500 °C, panel B; 600 °C, panel C; 700 °C, panel D) and ASR ([$\Omega \cdot cm^2$], 400 °C, panel E; 500 °C, panel F, 600 °C, panel G, 700 °C, panel H).

However, the substitution of a small amount of Ni (y = 0.2–0.4) for Co leads to slightly improved performance and significant TEC reduction, despite a decrease of the electrical conductivity, as demonstrated by the compounds synthesized by Kim et al. [117]. In this paper, the most promising compound is $NdBaCo_{1.6}Ni_{0.4}O_{5+\delta}$ that presents a TEC value of 16.9 10^6 K^{-1}, lower than the parent compound. Liu and coauthors [51] instead reported on the characterization of $PrBa_{0.5}Sr_{0.5}Co_{2-x}Ni_xO_{5+\delta}$ compounds (x = 0.1, 0.2, 0.3) and found a worsening of the ASR at increasing x. For what concerns the electrical conductivity instead, the general trend was to lower the conductivity, but due to a change in the slope, the sample with x = 0.3 showed a total electrical conductivity higher

Table 15
TECs of selected compounds as a function of Sr content.

x in $GdBa_{1-x}Sr_xCo_2O_{5+\delta}$	TEC [10^6 K^{-1}] (80–900 °C)	Reference
x = 0.0	16.6–20.8	[67–71]
x = 0.2	18.0	[67]
x = 0.4	18.3	
x = 0.6	19.5	
x = 1.0	18.8	

than the x = 0.1 sample in the temperature range below 550 °C. Even lower TEC values are achieved with $SmBaCo_{1.6}Ni_{0.4}O_{5+\delta}$ prepared by Che at al [50]. and with $GdBaCo_{1.7}Ni_{0.3}O_{5+\delta}$ by Wei at al. [71], that obtained TECs respectively equal to 16.6 and $15.5 \cdot 10^6$ K^{-1}.

5.2.3. Cu doping

An alternative to Fe doping is using Cu to substitute Co in B site of double perovskite, in order to achieve the best tradeoff between TEC and electrochemical performance. TEC values decrease monotonically with increasing Cu content up to y = 1. Several publications report a characterization of compounds with half Co substituted with Cu, leading to the conclusion that TEC is greatly reduced, but also the electrochemical parameters [31,43,72]. However, Zhang et al. [24] and Kim et al. [118] investigated more deeply on Cu content, synthesizing material series with increasing Cu content, $YBaCo_{2-y}Cu_yO_{5+\delta}$ (with y = 0, 0.2, 0.4, 0.6, 0.8) and $LnBaCo_{2-y}Cu_yO_{5+\delta}$ (with Ln = Gd and Nd and y = 0, 0.25, 0.5, 0.75, 1) respectively. Zhang et al. report the lowest ASR values (0.125 Ω cm^2 at 700 °C), among his doped materials for $YBaCo_{1.4}Cu_{0.6}O_{5+\delta}$ compound, and a very low TEC, equal to $14.7 \cdot 10^6$ K^{-1}. The TEC is even lower for y = 0.8 compound, but both present conductivity values below 100 S cm^{-1} in the intermediate temperature range (500–800 °C), not completely satisfying the requirements of a cathodic application. Similar trend is reported for material series produced and characterized by Kim et al.. TEC values are lowered by Cu content, and $NdBaCo_{1.25}Cu_{0.75}O_{5+\delta}$ (presenting TEC equal to $16.4 \cdot 10^6$ K^{-1}) and $GdBaCoCuO_{5+\delta}$ (TEC = $14.5 \cdot 10^6$ K^{-1}) samples show improved cathode performances compared to the Cu-free samples, considering maximum power density obtained in a complete cell. However, the measurements of conductivity and ASR show worsened values with increasing Cu content [118].

5.2.4. Sc doping

Of particular interest is a paper published by Li et al. [38], reporting the substitution of Co with Sc, in order to both reduce TEC and improve performance. This series of materials, $PrBaCo_{2-y}Sc_yO_{5+\delta}$ (with y = 0.05, 0.1, 0.2, 0.5), show that Sc doping leads to a decrease in both ASR and activation energies, and to a reduction of TEC values (from 23.6 at y = 0.05 to $19.8 \cdot 10^6$ K^{-1} at y = 0.5). However, conductivity values decrease in a significant extent with increasing Sc content, reaching values below 50 S cm^{-1} for $PrBaCo_{1.5}Sc_{0.5}O_{5+\delta}$. Despite these low conductivity values, Sc doping seems a promising strategy and deserves a deeper investigation, in order to clarify the enhancement of oxygen reduction reaction kinetics at high Sc content.

5.2.5. Mn doping

Using Mn as B site dopant resulted in one of the lowest TEC reported in literature for double perovskite materials containing Co [58]. Kim et al. prepared and characterized a series of $PrBa_{0.5}Sr_{0.5}Co_{2-y}Mn_yO_{5+\delta}$ compounds (y = 0, 0.25, 0.5), obtaining a TEC value of $14.3 \cdot 10^6$ K^{-1} for $PrBa_{0.5}Sr_{0.5}Co_{1.5}Mn_{0.5}O_{5+\delta}$. Although Mn doping reduces electrochemical parameters, at 600 °C the material with y = 0.5 maintains acceptable conductivity and ASR values for cathodic application: 717 S cm^{-1} and 0.156 Ω cm^2 respectively. In addition, this study shows also the possibility of producing composite cathodes mixing a cathodic material with an electrolyte one. A cathode made by mixing GDC and $PrBa_{0.5}Sr_{0.5}Co_{1.5}Mn_{0.5}O_{5+\delta}$ in a 50% weight ratio presents a TEC value equal to $11.7 \cdot 10^6$ K^{-1}, a number that completely matches with pure GDC electrolyte TEC ($11.4–12.5 \cdot 10^6$ K^{-1}).

5.3. Latest developments: vacancy doping of double perovskites

A very recent trend used to tailor electrochemical performance of double perovskite materials is to produce compounds with a deficient stoichiometry for element on A or A′ site. A′ site understoichiometry was first investigated: a small Ba deficiency (x = 0–0.08) in $PrBa_{1-x}Co_2O_{5+\delta}$ [86] caused a shrinkage of the crystal cell size, slightly affected the thermal expansion coefficient, and affected both the electrical conductivity the electrochemical activity. In details, the electrical conductivity decreased at x = 0.03, then increased at x = 0.05 and again up to x = 0.08, where it was higher than in the stoichiometric compound [86]. The electrochemical activity improved with the increasing of barium deficiency up to x = 0.08 and the activation energy decreased. The same compounds have been prepared by Wang et al. [119] and Dong et al. [120], reporting contrasting results. The main difference between those compounds is the synthesis method: Wang et al. synthesized the materials through solid state reaction, while Pang et al. and Dong et al. used sol–gel methods. By the way, even the latters reported contrasting trends in electrical conductivity as a function of Ba deficiency.

The main divergence resulted in conductivity values that, in the temperature range 600–700 °C vary from 250 to 300 S cm^{-1} [86] up to values much higher than 800 S cm^{-1} in Wang et al. [119] and Dong et al. [120] compounds. However, considering ASR, Pang et al.'s materials presented slightly higher values, but still reasonably comparable and suitable for cathodic application (0.093 Ω cm^2 at 600 °C for x = 0.08, 0.042 Ω cm^2 for x = 0.06). These results aroused interest in the A′ site deficiency, that seems to be a worthwhile route to enhance double perovskites electrochemical performance. The best results among the series produced have been achieved by Pang et al. with $PrBa_{0.92}Co_2O_{5+\delta}$ and by Wang et al. with $PrBa_{0.94}Co_2O_{5+\delta}$. A similar study was performed on $LaBa_{1-x}Co_2O_{5+\delta}$ [121]; this compound tolerated a larger understoichiometry (x = 0–0.15) without significant modification of the lattice parameters; however, even if ASR values monotonically improved by increasing the deficiency up to 10%, the electrical conductivity decreased drastically with Ba deficiency.

Improvement of the electrochemical activity was also found in $NdBa_{1-x}Co_2O_{5+\delta}$ (x = 0, 0.05, 0.10) [122]; the maximum accepted Ba deficiency is slightly lower than 10%. The Ba deficiency affects the cell dimensions by reduction of the b lattice parameter, and by increase of the mean oxidation state of Co and increase of the oxygen vacancies. Although the highest total electrical conductivity is met at a Ba deficiency equal to 5% (750 S cm^{-1} at 700 °C), ASR investigation revealed that the optimal electrocatalytic activity in the oxygen reduction process was realized by the compound with 10% Ba understoichiometry, where the ASR (0.1 Ω cm^2 at 700 °C) was tenfold reduced with respect to the stoichiometric compound. The same trends have been observed in the circumstance of an A site deficiency series of double perovskites ($Sm_{1-x}BaCo_2O_{5+\delta}$ with x = 0–0.08 [63]). These materials present a decrease in both conductivity and ASR values with increasing deficiency up to x = 0.05; this change in performance is accompanied by a growth in the size of the orthorhombic cell.

The results of these papers about deficient materials could all be rationalized by the interplay between the dominant charge compensation mechanism, as already mentioned in Section 4 for

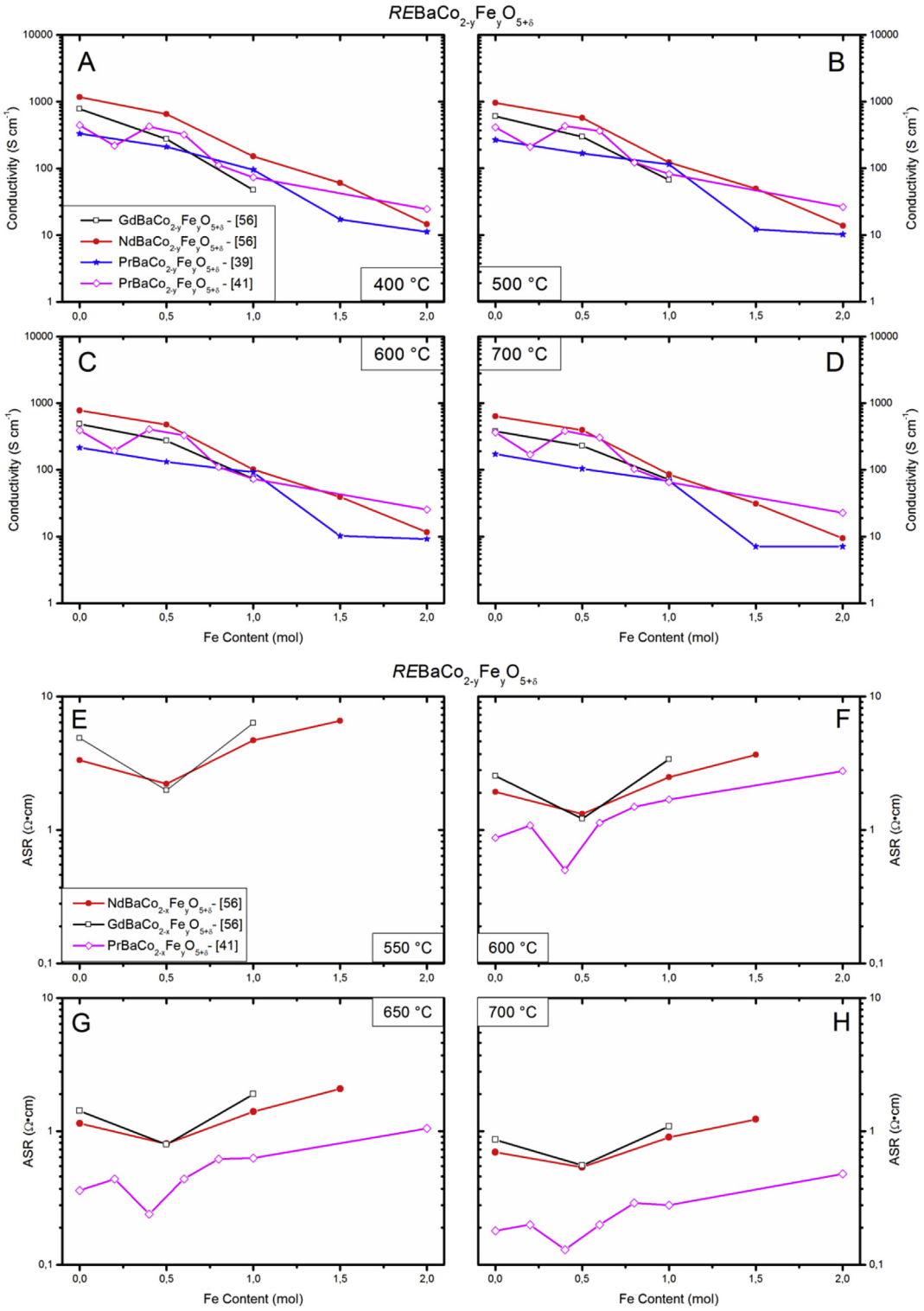

Fig. 7. Electrochemical characteristics of selected $RE BaCo_{2-y}Fe_yO_{5+\delta}$ compounds as a function of iron content y: total electrical conductivities σ ([S·cm^{-1}], 400 °C, panel A; 500 °C, panel B; 600 °C, panel C; 700 °C, panel D) and ASR ([Ω•cm^2], 550 °C, panel E; 600 °C, panel F, 650 °C, panel G, 700 °C, panel H).

doping elements. The introduction of deficiency generates metal ion vacancies, v''_{Ba} or v''_{RE}, that can be compensated by the generation of new electronic ($Co^{\bullet}_{Co}$) or ionic ($v^{\bullet\bullet}_{O}$) defects, that act as the charge carriers of electrons and ions. A similar effect can be found by changing the A:A′ ratio, while keeping the total occupancy of the two sites full, as in $Pr_{1+x}Ba_{1-x}Co_2O_{5+\delta}$ (x = 0–0.30): the most interesting result is the decrease of both the cathodic polarization resistance and the thermal expansion coefficient by increasing the amount of rare earth [37].

In conclusion, the deficiency seems to generally improve the electrochemical parameters, with different effects based on material structure. In addition, also a slight reduction of TEC has been

observed, even if it does not still appear as decisive for application 'as is' in combination with the common electrolytes.

6. Summary

Double perovskite compounds are promising materials for cathodic application in IT-SOFCs, due to their excellent chemical and electrochemical properties. This review proposed a detailed discussion about the general characteristics of *RE*$BaCo_2O_{5+\delta}$ compounds, reporting the main chemical, physical thermal and electrochemical parameters available in the literature, with a special focus on electrical conductivity σ, ASR and TEC.

These materials show very high electronic conductivities, while few data are available about their ionic conductivities. However, the ability to withstand a large concentration of oxygen vacancies is a fundamental characteristic of these double perovskites compounds. In order to optimize the performance of the cathode in the oxygen reduction reaction, the role of oxygen vacancies is crucial. The balance between electronic and ionic conductivities is related to the electron hopping pathway along the Co—O—Co bonds; in addition, some authors argue that the more regular the structure, the better is the overlapping between the Co and O orbitals, resulting in enhanced electronic conductivity. This is likely the main reason for the conductivity improvement when A′ site is partially doped with Sr. On the other hand, the ductility of the oxidation states of Cois also responsible of the very high TEC values; partially substituting Co with other metals mitigates this effect, but also worsen the electrochemical performance.

Finally, more accurate analyses would allow to clarify how the electrochemical performance are related to crystal structure and preparation conditions. A deep insight in the various phenomena affecting ASR (i.e. oxygen surface exchange, charge transfer, bulk and surface ion diffusion, gas-phase diffusion etc.) and conductivity (i.e. electronic and ionic conductivities) would be of help in understanding how to improve the performance. Many possibilities are still available to find solutions to actual SOFC technological issues.

References

[1] V. Kharton, F. Marques, A. Atkinson, Solid State Ion. 174 (2004) 135—149.
[2] A. Orera, P.R. Slater, Chem. Mater. 22 (2010) 675—690.
[3] K.D. Kreuer, Annu. Rev. Mater. Res. 33 (2003) 333—359.
[4] H.S. Spacil. 1970. US Patent 3,503,809. Filed October 30, 1964.
[5] J.A. Kilner, M. Burriel, Annu. Rev. Mater. Res. 44 (2014) 365—393.
[6] S. Tao, J.T.S. Irvine, A252, J. Electrochem. Soc. 151 (2004).
[7] S. Tao, P.I. Cowin, R. Lan, Novel anode materials for SOFC, in: Functional Materials for Sustainable Energy Applications, Woodhead Publishing, 2012, pp. 445—477.
[8] D. Singh, R. Singh, J. Chem. Sci. 122 (2010) 807—811.
[9] Y. Hu, Y. Bouffanais, L. Almar, A. Morata, A. Tarancon, G. Dezanneau, Int. J. Hydrogen Energy 38 (2013) 3064—3072.
[10] E.V. Tsipis, V.V. Kharton, J. Solid State Electrochem. 12 (2008) 1367—1391.
[11] E.V. Tsipis, V.V. Kharton, J. Solid State Electrochem. 12 (2007) 1039—1060.
[12] E.V. Tsipis, V.V. Kharton, J. Solid State Electrochem. 15 (2011) 1007—1040.
[13] A. Tarancón, M. Burriel, J. Santiso, S.J. Skinner, J.A. Kilner, J. Mater. Chem. 20 (2010) 3799.
[14] A.A. Taskin, A.N. Lavrov, Y. Ando, Appl. Phys. Lett. 86 (2005) 091910.
[15] N. Dasgupta, R. Krishnamoorthy, K. Thomas Jacob, Mater. Sci. Eng. B90 (2002) 278—286.
[16] K.T. Lee, A. Manthiram, Chem. Mater. 18 (2006) 1621—1626.
[17] A. Manthiram, J.-H. Kim, Y.N. Kim, K.-T. Lee, J. Electroceram. 27 (2011) 93—107.
[18] P.S. Anderson, C.A. Kirk, J. Knudsen, I.M. Reaney, A.R. West, Solid State Sci. 7 (2005) 1149—1156.
[19] A. Maignan, C. Martin, D. Pelloquin, N. Nguyen, B. Raveau, J. Solid State Chem. 142 (1999) 247—260.
[20] J.H. Kim, A. Manthiram, J. Electrochem. Soc. 155 (2008) B385.
[21] E.L. Rautama, V. Caignaert, P. Boullay, K. Asish Kundu, V. Pralong, M. Karppinen, C. Ritter, B. Raveau, Chem. Mater. 21 (2009) 102—109.
[22] H. Takahashi, F. Munakata, M. Yamanaka, Phys. Rev. B 57 (1998) 15211—15218.
[23] J.-H. Kim, Y.N. Kim, Z. Bi, A. Manthiram, M.P. Paranthaman, A. Huq, Solid State Ion. 253 (2013) 81—87.
[24] Y. Zhang, B. Yu, S. Lü, X. Meng, X. Zhao, Y. Ji, Y. Wang, C. Fu, X. Liu, X. Li, Y. Sui, J. Lang, J. Yang, Electrochim. Acta 134 (2014) 107—115.
[25] J. Xue, Y. Shen, T. He, J. Power Sources 196 (2011) 3729—3735.
[26] E. Chavez, M. Mueller, L. Mogni, A. Caneiro, J. Phys. Conf. Ser. 167 (2009) 012043.
[27] D. Muñoz-Gil, D. Pérez-Coll, J. Peña-Martínez, S. Garcia-Martín, J. Power Sources 263 (2014) 90—97.
[28] D. Akahoshi, Y. Ueda, J. Solid State Chem. 156 (2001) 355—363.
[29] K. Zhang, L. Ge, R. Ran, Z. Shao, S. Liu, Acta Mater. 56 (2008) 4876—4889.
[30] R. Pelosato, A. Donazzi, G. Dotelli, C. Cristiani, I. Natali Sora, M. Mariani, J. Eur. Ceram. Soc. 34 (2014) 4257—4272.
[31] Q. Zhou, T. He, Q. He, Y. Ji, Electrochem. Commun. 11 (2009) 80—83.
[32] Q. Zhou, W.C.J. Wei, Y. Guo, D. Jia, Electrochem. Commun. 19 (2012) 36—38.
[33] J.H. Kim, L. Mogni, F. Prado, A. Caneiro, J.A. Alonso, A. Manthiram, J. Electrochem. Soc. 156 (2009) B1376.
[34] F. Jin, Y. Shen, R. Wang, T. He, J. Power Sources 234 (2013) 244—251.
[35] R.A. Cox-Galhotra, S. McIntosh, Solid State Ion. 228 (2012) 14—18.
[36] H. Zhao, Y. Zheng, C. Yang, Y. Shen, Z. Du, K. Świerczek, Int. J. Hydrogen Energy 38 (2013) 16365—16372.
[37] L. Jiang, F. Li, T. Wei, R. Zeng, Y. Huang, Electrochim. Acta 133 (2014) 364—372.
[38] X. Li, X. Jiang, H. Xu, Q. Xu, L. Jiang, Y. Shi, Q. Zhang, Int. J. Hydrogen Energy 38 (2013) 12035—12042.
[39] L. Zhao, J. Shen, B. He, F. Chen, C. Xia, Int. J. Hydrogen Energy 36 (2011) 3658—3665.
[40] W. Wang, T.S. Peh, S.H. Chan, T.S. Zhang, ECS Trans. 25 (2009) 2277—2281.
[41] J. Zou, J. Park, B. Kwak, H. Yoon, J. Chung, Solid State Ion. 206 (2012) 112—119.
[42] S. Park, S. Choi, J. Kim, J. Shin, G. Kim, ECS Electrochem. Lett. 1 (2012) F29—F32.
[43] L. Zhao, Q. Nian, B. He, B. Lin, H. Ding, S. Wang, R. Peng, G. Meng, X. Liu, J. Power Sources 195 (2010) 453—456.
[44] F. Jin, H. Xu, W. Long, Y. Shen, T. He, J. Power Sources 243 (2013) 10—18.
[45] S. Choi, S. Yoo, J. Kim, S. Park, A. Jun, S. Sengodan, J. Kim, J. Shin, H.Y. Jeong, Y. Choi, G. Kim, M. Liu, Sci. Rep. 3 (2013) 1—6.
[46] S. Lü, G. Long, X. Meng, Y. Ji, B. Lü, H. Zhao, Int. J. Hydrogen Energy 37 (2012) 5914—5919.
[47] J.H. Kim, M. Cassidy, J.T.S. Irvine, J. Bae, J. Electrochem. Soc. 156 (2009) B682.
[48] A.K. Azad, J.H. Kim, J.T.S. Irvine, J. Power Sources 196 (2011) 7333—7337.
[49] L. Jiang, T. Wei, R. Zeng, W.-X. Zhang, Y.-H. Huang, J. Power Sources 232 (2013) 279—285.
[50] X. Che, Y. Shen, H. Li, T. He, J. Power Sources 222 (2013) 288—293.
[51] L. Liu, R. Guo, S. Wang, Y. Yang, D. Yin, Ceram. Int. 40 (2014) 16393—16398.
[52] J.H. Kim, J.T.S. Irvine, Int. J. Hydrogen Energy 37 (2012) 5920—5929.
[53] T.V. Aksenova, L.Y. Gavrilova, D.S. Tsvetkov, V.I. Voronin, V.A. Cherepanov, Russ. J. Phys. Chem. A 85 (2011) 427—432.
[54] T.V. Aksenova, L.Y. Gavrilova, A.A. Yaremchenko, V.A. Cherepanov, V.V. Kharton, Mater. Res. Bull. 45 (2010) 1288—1292.
[55] S. Yoo, S. Choi, J. Kim, J. Shin, G. Kim, Electrochim. Acta 100 (2013) 44—50.
[56] Y.N. Kim, J.H. Kim, A. Manthiram, J. Power Sources 195 (2010) 6411—6419.
[57] M. West, A. Manthiram, Int. J. Hydrogen Energy 38 (2013) 3364—3372.
[58] J. Kim, S. Choi, S. Park, C. Kim, J. Shin, G. Kim, Electrochim. Acta 112 (2013) 712—718.
[59] F. Jin, L. Li, T. He, J. Power Sources 273 (2015) 591—599.
[60] A.C. Tomkiewicz, M. Meloni, S. McIntosh, Solid State Ion. 260 (2014) 55—59.
[61] A. Jun, J. Kim, J. Shin, G. Kim, Int. J. Hydrogen Energy 37 (2012) 18381—18388.
[62] N.E. Volkova, L.Y. Gavrilova, V.A. Cherepanov, T.V. Aksenova, V.A. Kolotygin, V.V. Kharton, J. Solid State Chem. 204 (2013) 219—223.
[63] X. Jiang, Q. Xu, Y. Shi, X. Li, W. Zhou, H. Xu, Q. Zhang, Int. J. Hydrogen Energy 39 (2014) 10817—10823.
[64] Y. Wang, X. Zhao, S. Lü, X. Meng, Y. Zhang, B. Yu, X. Li, Y. Sui, J. Yang, C. Fu, Y. Ji, Ceram. Int. 40 (2014) 11343—11350.
[65] J.H. Kim, M. Cassidy, J.T.S. Irvine, J. Bae, Chem. Mater. 22 (2010) 883—892.
[66] K. Zheng, K. Świerczek, J. Bratek, A. Klimkowicz, Solid State Ion. 262 (2014) 354—358.
[67] J.H. Kim, F. Prado, A. Manthiram, J. Electrochem. Soc. 155 (2008) B1023.
[68] A. Chang, S. Skinner, J. Kilner, Solid State Ion. 177 (2006) 2009—2011.
[69] A. Tarancón, S.J. Skinner, R.J. Chater, F. Hernández-Ramírez, J.A. Kilner, J. Mater. Chem. 17 (2007) 3175.
[70] L. Mogni, F. Prado, C. Jiménez, A. Caneiro, Solid State Ion. 240 (2013) 19—28.
[71] B. Wei, Z. Lü, D. Jia, X. Huang, Y. Zhang, W. Su, Int. J. Hydrogen Energy 35 (2010) 3775—3782.
[72] S.H. Jo, P. Muralidharan, D.K. Kim, Electrochem. Commun. 11 (2009) 2085—2088.
[73] C. Kuroda, K. Zheng, K. Świerczek, Int. J. Hydrogen Energy 38 (2013) 1027—1038.
[74] J. Kim, A. Jun, J. Shin, G. Kim, J. Stevenson, J. Am. Ceram. Soc. 97 (2013) 651—656.
[75] Q. Zhou, T. Wei, S. Guo, X. Qi, R. Ruan, Y. Li, Y. Wu, Q. Liu, Ceram. Int. 38 (2012) 2899—2903.
[76] F. Meng, T. Xia, J. Wang, Z. Shi, J. Lian, H. Zhao, J.-M. Bassat, J.-C. Grenier, Int. J. Hydrogen Energy 39 (2014) 4531—4543.
[77] X. Zhang, H. Hao, Q. He, X. Hu, Phys. B Condens. Matter 394 (2007) 118—121.

[78] A. McKinlay, J. Phys. Chem. C 111 (2007) 19120–19125.
[79] S. Lü, B. Yu, X. Meng, Y. Zhang, Y. Ji, C. Fu, L. Yang, X. Li, Y. Sui, J. Yang, Ceram. Int. 40 (2014) 14919–14925.
[80] Y.Q. Jia, J. Solid State Chem. 95 (1991) 184–187.
[81] R.D. Shannon, Acta Crystallogr. 32A (1976) 751–767.
[82] B.C.H. Steele, Solid State Ion. 134 (2000) 3–20.
[83] K.K. Hansen, K.V. Hansen, Solid State Ion. 178 (2007) 1379–1384.
[84] G.C. Kostogloudis, C. Ftikos, Solid State Ion. 126 (1999) 143–151.
[85] Z. Liu, L.-z. Cheng, M.-F. Han, J. Power Sources 196 (2011) 868–871.
[86] S. Pang, X. Jiang, X. Li, Q. Wang, Z. Su, J. Power Sources 204 (2012) 53–59.
[87] G. Yang, J. Feng, W. Sun, N. Dai, M. Hou, X. Hao, J. Qiao, K. Sun, J. Power Sources 268 (2014) 771–777.
[88] W. Zhou, R. Ran, Z. Shao, W. Jin, N. Xu, J. Power Sources 182 (2008) 24–31.
[89] S.B. Adler, Solid State Ion. 111 (1998) 125–134.
[90] D. Chen, R. Ran, Z. Shao, J. Power Sources 195 (2010) 4667–4675.
[91] B. Wei, Z. Lü, W. Jiang, X. Zhu, W. Su, Electrochim. Acta 134 (2014) 136–142.
[92] D. Han, H. Wu, J. Li, S. Wang, Z. Zhan, J. Power Sources 246 (2014) 409–416.
[93] D. Chen, R. Ran, Z. Shao, J. Power Sources 195 (2010) 7187–7195.
[94] D. Chen, R. Ran, K. Zhang, J. Wang, Z. Shao, J. Power Sources 188 (2009) 96–105.
[95] S. Carter, A. Selcuk, R.J. Chater, J. Kajda, J.A. Kilner, B.C.H. Steele, Solid State Ion. 53–56 (1992) 597–605.
[96] F.A. Kröger, H.J. Vink, Solid State Phys. 3 (1956) 307–435.
[97] J.M. Ralph, C.c. Rossignol, R. Kumar, J. Electrochem. Soc. 150 (2003). A1518.
[98] C. Rossignol, J.M. Ralph, J. Bae, J.T. Vaughey, Solid State Ion. 175 (2004) 59–61.
[99] A. Tarancon, J. Penamartinez, D. Marrerolopez, A. Morata, J. Ruizmorales, P. Nunez, Solid State Ion. 179 (2008) 2372–2378.
[100] Q. Zhou, F. Wang, Y. Shen, T. He, J. Power Sources 195 (2010) 2174–2181.
[101] F. Tietz, Ionics 5 (1999) 129–139.
[102] W. Zając, K. Świerczek, J. Molenda, J. Power Sources 173 (2007) 675–680.
[103] S. Park, S. Choi, J. Shin, G. Kim, Electrochim. Acta 125 (2014) 683–690.
[104] M. Hou, W. Sun, P. Li, J. Feng, G. Yang, J. Qiao, Z. Wang, D. Rooney, J. Feng, K. Sun, J. Power Sources 272 (2014) 759–765.
[104] J. Xue, Y. Shen, T. He, Int. J. Hydrogen Energy 36 (2011) 6894–6898.
[105] V. Dusastre, J.A. Kilner, Solid State Ion. 126 (1999) 163–174.
[106] Y. Leng, S. Chan, Q. Liu, Int. J. Hydrogen Energy 33 (2008) 3808–3817.
[107] E. Perry-Murray, S.A. Barnett, Solid State Ion. 143 (2001) 265–273.
[109] P. Costamagna, M. Panizza, G. Cerisola, A. Barbucci, Electrochim. Acta 47 (2002) 1079–1089.
[110] X.J. Chen, K.A. Khor, S.H. Chan, L.G. Yu, Mater. Sci. Eng. A335 (2002) 246–252.
[111] D. Chen, Z. Lin, H. Zhu, R.J. Kee, J. Power Sources 191 (2009) 240–252.
[112] P. Costamagna, P. Costa, V. Antonucci, Electrochim. Acta 43 (1998) 375–394.
[113] V.M. Janardhanan, V. Heuveline, O. Deutschmann, J. Power Sources 178 (2008) 368–372.
[114] N.S. Tsvetkova, A.Y. Zuev, D.S. Tsvetkov, J. Power Sources 243 (2013) 403–408.
[115] E. Suard, F. Fauth, V. Caignaert, I. Mirebeau, G. Baldinozzi, Phys. Rev. B 61 (2000) R11871–R11874.
[116] C.-Y. Yoo, J.H. Joo, H.J. Lee, J.H. Yu, Mater. Lett. 108 (2013) 65–68.
[117] J.H. Kim, A. Manthiram, Electrochim. Acta 54 (2009) 7551–7557.
[118] Y.N. Kim, A. Manthiram, J. Electrochem. Soc. 158 (2011) B276.
[119] J. Wang, F. Meng, T. Xia, Z. Shi, J. Lian, C. Xu, H. Zhao, J.-M. Bassat, J.-C. Grenier, Int. J. Hydrogen Energy 39 (2014) 18392–18404.
[120] F. Dong, M. Ni, Y. Chen, D. Chen, M.O. Tade, Z. Shao, J. Mater. Chem. A 2 (2014) 20520–20529.
[121] S.L. Pang, X.N. Jiang, X.N. Li, H.X. Xu, L. Jiang, Q.L. Xu, Y.C. Shi, Q.Y. Zhang, J. Power Sources 240 (2013) 54–59.
[122] A. Donazzi, R. Pelosato, G. Cordaro, D. Stucchi, C. Cristiani, G. Dotelli, I. Natali Sora, Unpublished results, (2015).